2012

Global burned area and biomass burning emissions from small fires

J. T. Randerson
University of California - Irvine, jranders@uci.edu

Y. Chen
University of California - Irvine

G. R. van der Werf
VU University Amsterdam

B. M. Rogers
University of California - Irvine

D. C. Morton
Biospheric Sciences Branch, NASA Goddard Space Flight Center

Global burned area and biomass burning emissions from small fires

J. T. Randerson,[1] Y. Chen,[1] G. R. van der Werf,[2] B. M. Rogers,[1] and D. C. Morton[3]

Received 9 July 2012; revised 10 October 2012; accepted 11 October 2012; published 11 December 2012.

[1] In several biomes, including croplands, wooded savannas, and tropical forests, many small fires occur each year that are well below the detection limit of the current generation of global burned area products derived from moderate resolution surface reflectance imagery. Although these fires often generate thermal anomalies that can be detected by satellites, their contributions to burned area and carbon fluxes have not been systematically quantified across different regions and continents. Here we developed a preliminary method for combining 1-km thermal anomalies (active fires) and 500 m burned area observations from the Moderate Resolution Imaging Spectroradiometer (MODIS) to estimate the influence of these fires. In our approach, we calculated the number of active fires inside and outside of 500 m burn scars derived from reflectance data. We estimated small fire burned area by computing the difference normalized burn ratio (dNBR) for these two sets of active fires and then combining these observations with other information. In a final step, we used the Global Fire Emissions Database version 3 (GFED3) biogeochemical model to estimate the impact of these fires on biomass burning emissions. We found that the spatial distribution of active fires and 500 m burned areas were in close agreement in ecosystems that experience large fires, including savannas across southern Africa and Australia and boreal forests in North America and Eurasia. In other areas, however, we observed many active fires outside of burned area perimeters. Fire radiative power was lower for this class of active fires. Small fires substantially increased burned area in several continental-scale regions, including Equatorial Asia (157%), Central America (143%), and Southeast Asia (90%) during 2001–2010. Globally, accounting for small fires increased total burned area by approximately by 35%, from 345 Mha/yr to 464 Mha/yr. A formal quantification of uncertainties was not possible, but sensitivity analyses of key model parameters caused estimates of global burned area increases from small fires to vary between 24% and 54%. Biomass burning carbon emissions increased by 35% at a global scale when small fires were included in GFED3, from 1.9 Pg C/yr to 2.5 Pg C/yr. The contribution of tropical forest fires to year-to-year variability in carbon fluxes increased because small fires amplified emissions from Central America, South America and Southeast Asia—regions where drought stress and burned area varied considerably from year to year in response to El Nino-Southern Oscillation and other climate modes.

Citation: Randerson, J. T., Y. Chen, G. R. van der Werf, B. M. Rogers, and D. C. Morton (2012), Global burned area and biomass burning emissions from small fires, *J. Geophys. Res.*, *117*, G04012, doi:10.1029/2012JG002128.

1. Introduction

[2] Quantitative estimates of contemporary burned area are needed to address many ecological and Earth science challenges, including understanding disturbance-driven changes in ecosystem function and carbon fluxes [*Luo and Weng*, 2011], the impacts of land use on atmospheric chemistry and human health [*Johnston et al.*, 2012], and the strength of climate-carbon cycle feedbacks during the twenty-first century [e.g., *Golding and Betts*, 2008; *Kloster et al.*, 2012]. Global-scale burned area products are generated using change detection algorithms applied to time series of surface reflectance from moderate resolution spectrometers, typically at 500 m to 1 km resolution, and require calibration and

[1]Department of Earth System Science, University of California, Irvine, California, USA.
[2]Faculty of Earth and Life Sciences, VU University Amsterdam, Amsterdam, Netherlands.
[3]Biospheric Sciences Branch, NASA Goddard Space Flight Center, Greenbelt, Maryland, USA.

Corresponding author: J. T. Randerson, Department of Earth System Science, University of California, 3212 Croul Hall, Irvine, CA 92697, USA. (jranders@uci.edu)

0148-0227/12/2012JG002128

validation with higher resolution imagery [*Roy et al.*, 1999; *Stroppiana et al.*, 2003; *Silva et al.*, 2003; *Tansey et al.*, 2004; *Simon et al.*, 2004; *Roy et al.*, 2005; *Loboda et al.*, 2007; *Tansey et al.*, 2008; *Giglio et al.*, 2009; *Roy and Boschetti*, 2009]. Burned area time series have been used as drivers of biogeochemical and fuel load models, often following the conceptual framework developed by *Seiler and Crutzen* [1980], to estimate carbon emissions and other trace gas and aerosol fluxes [*Scholes et al.*, 1996; *Barbosa et al.*, 1999; *Amiro et al.*, 2001; *Hoelzemann et al.*, 2004; *Korontzi et al.*, 2004; *Mouillot and Field*, 2005; *Wiedinmyer et al.*, 2006; *Ito et al.*, 2008; *Schultz et al.*, 2008; *Reid et al.*, 2009; *van der Werf et al.*, 2010; *French et al.*, 2011; *Turetsky et al.*, 2011]. With this approach, information on fuels and combustion completeness must come from other sources, including field observations, satellite maps of vegetation cover, or model estimates.

[3] Studies evaluating contemporary fire trends often make use of another complementary source of information: measurements of active fires derived from visible and infrared radiation emitted directly by fire fronts during the time of a satellite overpass [*Dozier*, 1981; *Matson and Dozier*, 1981]. Several commonly used active fire products rely on anomalously high brightness temperatures observed in a middle infrared spectral band (near 4 μm) to detect fires, and use additional information from visible, near infrared, and thermal infrared bands to separate fires from sun glint, clouds, and high land surface temperatures [*Giglio et al.*, 2000; *Giglio et al.*, 2003; *Xu et al.*, 2010]. Active fires by themselves allow for the detection of the presence or absence of fire in a given pixel during an individual satellite overpass or sampling interval. When aggregated temporally and spatially, active fires allow for the quantification of temporal and spatial patterns [*Prins and Menzel*, 1992; *Kasischke and French*, 1995; *Scholes et al.*, 1996; *Giglio et al.*, 2006a; *Giglio*, 2007; *Chuvieco et al.*, 2008; *Zhang and Kondragunta*, 2008; *Roberts et al.*, 2009], multiyear trends [*Prins and Menzel*, 1994; *Aragao and Shimabukuro*, 2010; *Arino et al.*, 2012], relationships between fires and climate drivers [*Spessa et al.*, 2005; *van der Werf et al.*, 2008], and investigations of socioeconomic and cultural factors that influence fire use in different countries [*Mollicone et al.*, 2006; *Bowman et al.*, 2011; *Lin et al.*, 2012].

[4] Additional information on fire radiative power (FRP), the rate of electromagnetic energy released by fire, is available for some satellite spectroradiometers whose detectors allow for accurate quantification of fire temperatures. Since the energy content of dry biomass does not vary considerably across different plant species, ecosystem type, or fuel type [*Pooter and Villar*, 1997; *Chapin et al.*, 2002], FRP measurements may enable direct estimates of fuel consumption, if they can be integrated through time to obtain estimates of fire radiative energy (FRE) [*Ellicott et al.*, 2009; *Vermote et al.*, 2009; *Freeborn et al.*, 2011]. This relatively direct approach for estimating emissions may shortcut some of the uncertainties associated with biogeochemical model estimates of fuel loads and combustion completeness [*Kaufman et al.*, 1998; *Wooster et al.*, 2003], yet presents its own challenges [*Kaiser et al.*, 2012].

[5] Burned area and active fire/FRP products both have strengths and weaknesses with respect to their use in developing a global time series of fire carbon emissions [*Roberts et al.*, 2011]. Burned area is likely to be less sensitive to variability in cloud cover and smoke in many regions since change detection algorithms can draw upon multiple satellite overpasses to obtain cloud-free scenes before and after a fire event. Burned area also provides direct estimate of final fire size and thus the total area experiencing emissions losses, enabling immediate use with models following the *Seiler and Crutzen* [1980] paradigm. Contemporary global burned area products have a limitation, however, because they are made using moderate resolution surface reflectance imagery, with pixel areas varying between 21 ha and approximately 100 ha [*Roy et al.*, 2005; *Loboda et al.*, 2007; *Tansey et al.*, 2008; *Giglio et al.*, 2009]. In some biomes there is accumulating evidence that many individual burn scars have sizes that are below the detection limit of these products [*Eva and Lambin*, 1998; *Laris*, 2005; *McCarty et al.*, 2009; *Roy and Boschetti*, 2009].

[6] Small fires often occur in agricultural settings where the size of an individual field limits the fire spread [*McCarty et al.*, 2009], where the use of prescribed fires is important for ecosystem management [e.g., *Covington et al.*, 1997], where wildland fires are suppressed near human settlements [*DeWilde and Chapin*, 2006], in ecosystems with heterogeneous patches of land cover that limit the continuity of dry fuels [*Eva and Lambin*, 1998; *Laris*, 2005], and in places and times where fuel moisture and atmospheric conditions do not sustain high fire spread rates [*Van Wagner*, 1977; *Hély et al.*, 2001]. In the U.S., for example, agricultural field sizes vary by region, with an average of approximately 16 ha in many southern and eastern regions [*McCarty et al.*, 2009]. Assuming that agricultural fires burn individual fields, this places a regionally varying upper bound on fire sizes detectable from satellite imagery. Developing calibration or validation estimates of burned area associated with many of the agricultural and prescribed fires described above for remote sensing-derived products is made difficult because few state and national programs systematically quantify this type of burned area with high levels of accuracy. Further, since several burned area detection algorithms require that a substantial fraction of an individual pixel's area undergo burning for successful attribution (to avoid commission errors from other forms of land cover change), detection of these sub-pixel fires can be difficult [*Roy and Landmann*, 2005; *Roy and Boschetti*, 2009]. As a result, the contribution of small fires to continental and global-scale scale patterns of burned area and carbon emissions remains poorly understood.

[7] Active fire products have unique properties that may provide new information about small fire contributions to burned area and emissions. Specifically, these products have the advantage of enabling the detection of fires that are considerably smaller than the spatial resolution of an individual moderate resolution surface reflectance pixel because of the strong nonlinearity in radiative power as a function of fire temperature [*Giglio et al.*, 2003]. For example, the 1-km MODIS active fire product has a 50% detection efficacy for fires in different vegetation types that span approximately 25 to 70 actively burning 30 m Advanced Spaceborne Thermal Emission and Reflection Radiometer (ASTER) pixels [*Morisette et al.*, 2005; *Csiszar et al.*, 2006; *Schroeder et al.*, 2008]. This area is equivalent to approximately 10% to 30% of a 21.5 ha nadir MODIS surface reflectance pixel. Given that actively burning fire fronts are not expected to

completely cover the area of many ASTER fire pixels, the detection limit for MODIS probably is even higher—and more consistent with the area estimates from *Giglio et al.* [2003] based on spectroradiometer sensitivities.

[8] The relatively high sensitivity of the MODIS active fire product to small flaming fronts within each pixel makes it potentially useful for quantifying the spatial and temporal distribution of small fires at a global scale. The challenge, however, from the perspective of developing a biomass burning emissions time series is that this product provides only a relative measure of fire activity. Integration of FRP to FRE from MODIS, for example, requires accounting for gaps created by clouds and orbital geometry, estimating the diurnal cycle of FRP during periods in between satellite overpasses, adjusting for variable detection efficiencies as a function of scan angle, and removing the effects from commission errors [*Freeborn et al.*, 2009; *Freeborn et al.*, 2011]. An additional challenge with respect to the use of FRP involves uncertainties related to the dissipation of fire energy in sensible, latent, and radiant forms. Radiant energy is only a small fraction of the immediate energy release from a fire [*Wooster et al.*, 2005], and important uncertainties remain with respect to understanding how this fraction varies between different types of fires (i.e., flaming versus smoldering) and levels of fuel moisture [*Freeborn et al.*, 2011].

[9] Here we combined information from active fires and a 500 m burned area product to estimate the contribution of small fires to global biomass burning carbon emissions. In our approach, we tracked the difference normalized burn ratio (dNBR) [*López Garcia and Caselles*, 1991; *van Wagtendonk et al.*, 2004] for all active fire pixels inside and outside of burned areas in the 2001–2010 MODIS record, separately compiling statistics as a function of vegetation type, continental-scale region, seasonal period, and year. These data were then used to estimate the burned area associated with active fires located outside of the *Giglio et al.* [2009] burned area product. We hereafter refer to this set of burned area as the 'small fire' burned area because sub-500 m fires are likely to be a primary cause of active fires residing outside of the burned area product in many biomes, including agriculture, wooded savannas, and tropical forests. We evaluated our approach using FRP observations and several higher spatial resolution burned area products from North America, Europe, and Africa. To quantify uncertainties, we performed five sensitivity studies in which we modified key aspects of our approach or used different remote sensing data products to estimate small fire burned area. In a final step we investigate the impacts of including the burned area from these small fires on global fire emissions using the biogeochemical model from the Global Fire Emissions Database version 3 (GFED3) [*van der Werf et al.*, 2010]. We show that accounting for small fires considerably increased the total amount and interannual variability of carbon emissions from tropical forest regions.

2. Methods

2.1. Data Products

[10] We used the MCD64A1 burned area product [*Giglio et al.*, 2009] and the Collection 5 Level 3 daily composition thermal anomaly/fire product MOD14A1 (from NASA's Terra satellite) [*Giglio et al.*, 2003; *Morisette et al.*, 2005; *Csiszar et al.*, 2006; *Giglio et al.*, 2006a; *Schroeder et al.*, 2008; *Giglio*, 2010] in our primary analysis. The Aqua daily composition thermal anomaly/fire product (MYD14A1) was used in sensitivity tests described below. The MCD64A1 burned area product has a 500 m spatial resolution and monthly temporal resolution, although each file specifies the individual day of burning for every burned area pixel and a temporal uncertainty range for its burn date. The spatial and temporal coverage of the MCD64A1 burned area reported here is significantly greater than that used by *Giglio et al.* [2010] or subsequently by *van der Werf et al.* [2010] in GFED3: we used an updated version that included more than 98% of all MODIS land tiles during 2001–2010. Compared with GFED3, this updated set of burned area had the same global mean (345 Mha/yr during 2001–2010) but different regional patterns, with decreases in Central, Southeast, and Equatorial Asia, and increases in Central America and Northern Hemisphere South America. The two thermal anomaly (active fire) products from Terra and Aqua have a 1-km spatial resolution, report the presence or absence of fire each day during one or more daytime and nighttime overpasses, and include additional information about the confidence level of the retrieval, cloud or water cover, scan angle, and fire radiative power. Both the burned area and active fire products are defined on the MODIS sinusoidal grid.

[11] We excluded pixels with persistent non-fire hot spots from the MODIS daily composition thermal anomaly/fire products (MOD14A1 and MYD14A1) using a location database developed by *Csiszar et al.* [2006], gas flare pixels identified using the NOAA Global Gas Flare Estimates database [*Elvidge et al.*, 2009] (Google kmz files downloaded from www.ngdc.noaa.gov/dmsp/interest/gas_flares.html on 9 Mar 2010), and volcano locations from the NOAA National Geophysical Data Center (NGDC) Volcano Data and Information (Significant Volcanic Eruptions Database downloaded from www.ngdc.noaa.gov/hazard/volcano.shtml on 23 September 2011).

[12] As described below, we calculated dNBR for each active fire detection in the Terra time series using surface reflectance observations from the Vegetation Indices 16-day L3 (MOD13A1) collection 5 product [*Huete et al.*, 2002]. We chose Terra over Aqua for the surface reflectance time series because of its longer temporal coverage and we chose the 16-day vegetation indices (MOD13A1) product over the 8-day surface reflectance (MOD09A1) product because of the additional cloud screening provided by maximum compositing in the vegetation indices product. NBR is defined as (NIR-SWIR)/(NIR + SWIR) following *van Wagtendonk et al.* [2004] where NIR represents surface reflectance from a near infrared band and SWIR represents surface reflectance from a shortwave infrared band. For NIR we used band 2 and for SWIR we used band 7 from MOD13A1. Terra MODIS sensor degradation that impacts collection 5 surface reflectance estimates in visible wavelengths [*Wang et al.*, 2012] does not impact the longer wavelength bands used in this study. We computed the difference in NBR (dNBR) using the two NBR values immediately before and immediately after each active fire detection (and thus excluding the 16-day interval containing the day of the active fire detection to limit complications from the evolving burned area and smoke aerosols). The MOD13A1 product has a 500 m spatial resolution, and so NBR values for each set of 4 pixels corresponding to a single 1-km active fire pixel were averaged together for the

pre-fire and post-fire periods prior to computing dNBR. We used only surface reflectance pixels that had the highest quality retrievals—this included the set where the pixel reliability flag was equal to 0 (use with confidence) and the quality flag was equal to 00 (good quality). As described below, we also conducted a sensitivity test in which we computed dNBR for 2010 using the Surface Reflectance Bands 1–7 (MOD09A1) collection 5 product.

2.2. Small Fire Estimation

[13] To estimate monthly burned area in each 0.25° × 0.25° land grid cell (approximately 28 km × 28 km at the equator), we used the following equations:

$$BA_{total}(i,t,v) = BA_{MCD64A1}(i,t,v) + BA_{sf}(i,t,v), \quad (1)$$

where the total burned area, BA_{total}, in each grid cell, i, month t, and aggregated vegetation class, v, is the sum of the original MCD64A1 burned area, $BA_{MCD64A1}$, and a new component associated with small fires, BA_{sf}. As described below, our approach for estimating BA_{sf} was statistical, and required information about the ratio of active fires in or near large burned areas to active fires outside of these areas. Our choice of the 0.25° grid and the averaging system for model parameters described below reflected a balance between our goal of providing relatively high spatial resolution information for investigating regional to global scale Earth system science questions, and the requirements for maintaining a robust computation approach.

[14] We estimated the small fire component as:

$$BA_{sf}(i,t,v) = FC_{out}(i,t,v) \times \alpha_{r,s,v,y} \times \gamma_{r,s,v,y}, \quad (2)$$

where FC_{out} is the total number of MOD14A1 active fires outside of burned areas in each 0.25° grid cell, α is the ratio of $BA_{MCD64A1}$ to active fire counts within or near the perimeter of these burned areas, and γ is a scalar that modifies the burned area associated with FC_{out} because these active fires often were associated with smaller burn scars compared to active fires within or near burned areas identified by the MODIS MCD64A1 product. Active fires within or near burned areas (the complement to FC_{out}) are hereafter referred to as FC_{in}. α and γ were separately estimated within each of 14 continental-scale regions (r) for 3 seasonal periods (s), for 5 aggregated vegetation classes (v), and for each year (y). A flow diagram showing how the different MODIS products were used to compute equation (2) is provided in the auxiliary material (Figure S1).[1]

[15] We computed FC_{out} by applying a 1-km buffer to the perimeter of MCD64A1 burned areas, and then counting the number of active fire detections outside of this area. FC_{in} was defined as the complement to FC_{out}, i.e., the active fires that overlap with MCD64A1 burned area or the surrounding buffer area. All the active fires within one month of the burn date were assigned to FC_{in}. α had units of km^2 per active fire and was defined for our best case estimate using MCD64A1 burned area and FC_{in} derived from the Terra MOD14A1 product. The spatial distribution of α was influenced by the efficacy of the burned area detection algorithm, the frequency of satellite overpasses, and aspects of fire behavior such as the rate of movement of the fire front [e.g., *Giglio et al.*, 2006b]. α in equation (2) is not directly comparable to α from *Giglio et al.* [2010] because here we used a subset of the active fires in each grid cell (only those associated with FC_{in}) to compute this ratio. We included the spatial buffer described above to allow for more conservative (smaller) estimates of FC_{out}. Preliminary analysis suggested that increasing the buffer radius would reduce FC_{out} and α, but would be at least partly compensated by increases in the γ term described below in our estimates of small fire burned area from equation (2).

[16] To better understand the sensitivity of equation (2) to different satellite and environmental conditions, it can be rewritten in the following form, by replacing α with $BA_{MCD64A1}/FC_{in}$ and rearranging terms.

$$BA_{sf}(i,t,v) = BA_{MCD64A1}(i,t,v) \times \frac{FC_{out}(r,s,v,y)}{FC_{in}(r,s,v,y)} \times \gamma_{r,s,v,y}, \quad (3)$$

Although this form was not used in our analysis and involves a different approach for averaging FC_{in} and FC_{out}, it is important for understanding the sensitivity of BA_{sf} to different processes. Specifically, the general form of our approach depends on the ratio of active fires detected inside and outside of burn perimeters in each region and not the absolute number of active fires detected outside of burn scars. This may make the technique less sensitive to regional variations in satellite overpass dynamics and cloud cover, since the impacts of these factors would be expected to have similar effects for FC_{in} and FC_{out}. Hereafter, when we refer to FC_{out} (and FC_{in}), we refer to the form of FC_{out} (i, t, v) described by equation (2).

[17] The γ in equation (2) was an additional unitless scalar applied to FC_{out} to account for the observation that the set of active fires in FC_{out} did not necessarily correspond to the same size distribution of burn scars as those in FC_{in}. Specifically, in many regions FC_{out} had smaller dNBR changes than FC_{in}, indicating that on average, individual FC_{out} active fires were associated with smaller burns. As described below in the results (section 3.5), FC_{out} also had lower values of FRP, indicating that the active fires were smaller in size or cooler. γ was estimated using the following equation:

$$\gamma(r,s,v,y) = \frac{dNBR_{out}(r,s,v,y) - dNBR_{control}(r,s,v,y)}{dNBR_{in}(r,s,v,y) - dNBR_{control}(r,s,v,y)}, \quad (4)$$

where $dNBR_{out}$ was the difference normalized burn ratio corresponding to FC_{out}, $dNBR_{in}$ was the same quantity but for FC_{in}, and $dNBR_{control}$ was derived using dNBR from nearby unburned regions (for the same period, aggregated vegetation class, region, and year). We note that our approach assumed that dNBR differences between FC_{in} and FC_{out}, each relative to the control, were linearly proportional to subpixel burned area. While not strictly valid, this assumption was not entirely unreasonable provided the associated reflectance changes were not excessively large [*Roy and Landmann*, 2005]. We also assumed that all of the dNBR differences were attributable to BA_{sf} rather than to a change in fire severity. This latter assumption was probably conservative with respect to the BA_{sf} values we report in the results. Specifically, if burn severity was lower (per m^2 of burned area) for small fires outside of MCD64A1 burned areas, then the small fire burned

[1] Auxiliary materials are available in the HTML. doi:10.1029/2012JG002128.

area fractions would have to be even higher to affect the same dNBR change (i.e., the γ applied in equation (2) would need to be larger and thus closer to a value of 1).

2.3. Global Application of Small Fire Burned Area Algorithm

[18] We computed α and γ for three different seasonal periods and five aggregated vegetation classes within 14 continental-scale regions each year. We defined early, mid, and late season periods relative to the 2001–2010 mean peak fire month that was derived for each region using MOD14A1 active fire observations. Early season was defined as 1–6 months prior to the peak fire month, middle season as the peak fire month, and late season as 1–5 months after the peak fire month. We chose this seasonal partitioning to separate active fires into three bins of roughly equal size, in terms of the number of active fires within each seasonal interval.

[19] We also defined five aggregated vegetation classes within each continental region using the International Geosphere-Biosphere Programme (IGBP) vegetation classification scheme in the Collection 5 MCD12Q1 global land cover type product [*Friedl et al.*, 2002; *Friedl et al.*, 2010]. All the forests (classes 1–5) were grouped together in one class as were closed and open shrublands, woody savannas, and savannas (classes 6–9). Grasslands (class 10) were considered another separate aggregated class. Croplands and cropland/natural vegetation mosaic types also were grouped together (classes 12 and 14). The remaining vegetation types, including permanent wetlands (class 11), urban or built up (13), snow and ice (15), and barren or sparsely vegetation (class 16) were combined into an 'other' aggregated vegetation class. We used 2009 land cover type data from collection 5 for this mapping and anticipate improved performance with future versions of this product that remove known biases in high latitude regions.

[20] The seasonal periods and aggregated vegetation classes described above allowed α and γ to capture some of the variability in environmental and ecosystem controls on fire behavior in each region, but were sufficiently coarse to allow for robust estimation of these parameters using available data.

[21] We then computed BA_{sf} using equation (2) with monthly varying values of FC_{out} in each 0.25° grid cell and the matrices of α and γ parameters described above that had dimensions of 10 years, 14 continental-scale regions, 3 seasonal periods, and 5 aggregated vegetation classes.

2.4. Estimation of Small Fire Burned Area During Gaps in the Burned Area (MCD64A1) Record

[22] Application of equation (2) was possible only when both burned area tiles (MCD64A1) and active fires (MOD14A1) products were available. During 2001–2010, less than 1% of active fires occurred in places and months when monthly burned area tiles were unavailable. Thus, the approach described in the previous section (using equation (2)) was the most common approach for estimating BA_{sf} during 2001–2010. Where MCD64A1 burned area tiles were not available (mostly in very high northern and southern latitudes and during a gap in June 2001), we could not estimate FC_{out}, and thus BA_{sf} in equation (2). For these periods and regions, we used the following extrapolation to estimate both BA_{sf} and the total burned area.

[23] First, we created matrices of the long-term mean values of α and γ averaged using available observations during 2001–2010. These matrices had dimensions of 14 continental-scale regions, 3 seasonal periods, and 5 aggregated vegetation classes. We hereafter refer to these climatological mean parameters as α_c and γ_c. We constructed an additional matrix, R_{out}, of the mean ratio FC_{out} to the sum of FC_{out} and FC_{in} with the same dimensions. To estimate burned area normally captured by MCD64A1 during months with gaps, we applied the following equation:

$$BA_{MCD64A1\,gap}(i,t,v) = FC_{total}(i,t,v) \times (1 - R_{out}(r,s,v)) \times \alpha_c(r,s,v), \quad (5)$$

where FC_{total} is the total number of active fires observed in each 0.25° grid cell in a given month, separated by the five aggregated vegetation classes, $1 - R_{out}$ is the mean fraction of FC_{total} that is within or near burned areas (this parameter varied by continental region, seasonal period, and aggregated vegetation class), and α_c is defined in the preceding paragraph.

[24] Similarly, we estimated the burned area associated with small fires during these gap periods using the following equation:

$$BA_{sf\,gap}(i,t,v) = FC_{total}(i,t,v) \times R_{out}(r,s,v) \times \alpha_c(r,s,v) \times \gamma_c(r,s,v), \quad (6)$$

where R_{out} was the mean fraction of FC_{total} associated with small fires (i.e., active fires outside of burned areas and varying by continental region, seasonal period, and aggregated vegetation class) and α_c and γ_c were climatological mean parameters that convert the product of FC_{total} and R_{out} to burned area. Note that the product of FC_{total} and R_{out} provides an estimate of FC_{out} during gaps, so that equation (6) has a form similar to that of equation (2). This extrapolation approach accounted for less than 1% of the burned area in the 2001–2010 BA_{sf} time series presented below in section 3.

2.5. Evaluation

[25] We compared BA_{total} from our approach with several regional burned area data sets derived from higher resolution satellite imagery and geographic information system (GIS) fire location and fire size data. In Alaska we used the point version of the Alaskan Large Fire Database (AKLFDB) developed by the Alaska Fire Service (http://fire.ak.blm.gov/predsvcs/maps.php) [*Kasischke et al.*, 2002] and the continental-scale polygon data set produced by the Monitoring Trends in Burn Severity (MTBS) project [*Eidenshink et al.*, 2007]. In Canada, we used the point version of the Canadian National Fire Database (CNFDB, http://cwfis.cfs.nrcan.gc.ca/en_CA/nfdb/pnt, version 20101210) developed by the Canadian Forest Service [*Amiro et al.*, 2001; *Parisien et al.*, 2006]. We masked out Manitoba during 2001–2004, Nova Scotia during 2010, and Newfoundland and Labrador during 2001–2010 since fires from these provinces had not yet been added to the national database. For all of these comparisons, we first created raster maps of the observations on the same 0.25° grid as BA_{sf} and BA_{total}.

[26] For the continental United States (CONUS), we separated fires into several components. For wildland fires, we used observations from MTBS. To compare with our MODIS estimates, we regridded the National MTBS Burned Area Boundaries Data set (http://www.mtbs.gov/index.html) shape file perimeters to annual gridded maps. The MTBS protocol is

to map all fires on federal and state lands greater than 202 ha (500 acres) in the east and greater than 404 ha (1000 acres) in the west, with the dividing east-west line along the eastern border of North Dakota, South Dakota, Nebraska, Kansas, Oklahoma, and Texas. Although MTBS does not exclude prescribed fires with this protocol, these contributions are relatively small and thus cumulative MTBS burned area estimates for the United States are very similar to wildland fire estimates reported by National Interagency Fire Center (NIFC) [*Eidenshink et al.*, 2007]. For agricultural burned area, we compared our estimates with the cropland product developed by *McCarty et al.* [2009]. The *McCarty et al.* [2009] estimates were available during 2003–2007 and were derived using regionally specific dNBR thresholds that were optimized based on 296 ground observations (GPS burn perimeters) from burned and plowed fields. To compare with these observations, we first calculated the amount of BA_{total}, BA_{sf}, and $BA_{MCD64A1}$ in CONUS that occurred in croplands and cropland/natural vegetation mosaic types using the 500 m MCD12Q1 global land cover product.

[27] In a final step of evaluation in CONUS, we compared our estimates with prescribed fires from NIFC [*NIFC*, 2012]. For this, we computed a residual component after removing burned area overlapping with MTBS fire scars and burned area in agricultural regions, following the methods described above. The NIFC prescribed fire statistics were available for individual states, and we compared these estimates with the MODIS-based burned area for CONUS as a whole and on a state-by-state basis.

[28] We also compared our estimates of $BA_{MCD64A1}$ and BA_{total} with aggregated burned area statistics derived from Landsat imagery from the National Forest service in Portugal (www.afn.min-agricultura.pt/portal/dudf/cartografia/cartografareas-ardidas-1990-2009) [e.g., *Marques et al.*, 2011] and a savanna region in southern Mali, Africa based on the study of *Laris* [2005]. For the Portugal data set, we created raster maps of the polygon information on the same 0.25° as BA_{sf}. For the Mali comparison, we extracted and averaged together all of the 0.25° grid cells during the 2002–2003 fire season within the Landsat ETM + scene WRS-199/52 that was the focus of the *Laris* [2005] analysis. In our validation, we attempted to use all publicly available regional burned area data that we could find. We recognize that these data sets are biased toward North America and anticipate increased availability of high quality burned area observations from many other continents in the future from Landsat as a part of ongoing Global Observation of Forest and Land Cover Dynamics (GOFC-GOLD) efforts and other activities.

2.6. Sensitivity Tests

[29] We also separately compared MODIS fire radiative power (FRP) of active fires outside of burned areas (FC_{out}) with those within or near burned areas (FC_{in}). Fire radiative power provides information about some combination of fire temperatures, flaming versus smoldering fire stages, and fire area within a 1-km MODIS pixel [*Freeborn et al.*, 2008; *Ichoku et al.*, 2003; *Wooster et al.*, 2003]. As described below in the results, these FRP comparisons indicated that active fires outside of burned areas were smaller and/or cooler. We did not use FRP directly to estimate γ because it remains uncertain how instantaneous fire behavior may be related to the final size of an individual fire.

[30] We also conducted several tests to evaluate the sensitivity of our results to different assumptions with our approach. These included 1) using 8-day surface reflectance (MOD09A1) to estimate dNBR instead of the 16-day vegetation index product described above; 2) constructing the dNBR control using a temporal sampling approach instead of the spatial sampling approach described above, 3) replacing Terra with Aqua active fires for the estimation of FC_{in}, FC_{out}, and α, 4) the same as 3 but also using Aqua surface reflectance to compute γ; and 5) only using nominal and high confidence active fire data to determine FC_{out}, α, and γ. For the temporal sampling estimate of $dNBR_{control}$, we obtained this estimate by sampling within burned area perimeters in the year prior to burning, and also by stratifying by aggregated vegetation class and seasonal period. For all five of these tests, we compared burned area estimates with results from our primary approach for the year 2010.

2.7. Carbon Emissions Modeling

[31] To test the impact of adding small fire burned area on emissions, we ran the GFED3 biogeochemical model [*van der Werf et al.*, 2010] with $BA_{MCD64A1}$ as well as with BA_{total}. Boosting burned area will increase emissions, but the relation is not necessarily linear for a number of reasons. First, it depends on where and when the small fires occur because 1) fuel loads vary considerably across the landscape as a function of vegetation type and 2) the fraction of fuels consumed (combustion completeness) varies through time as a function of fuel moisture levels. Second, if the increase in burned area occurs in areas with frequent fires, then the fuel loads may not have had time to recover from the previous fire, leading to proportionally smaller emissions increases.

[32] We completed two simulations at a 0.25° spatial resolution. All input data sets except burned area, fire persistence, and the fraction of burned area occurring in tropical peatlands were the same and were derived from the original 0.5° GFED3 runs described by *van der Werf et al.* [2010]. Within each 0.25° grid cell, we kept track of the sub-grid partitioning of the 500 m burned area for $BA_{MCD64A1}$ over different land cover classes, tree cover bins, and peatland maps [*van der Werf et al.*, 2010]. We did the same with BA_{sf} by tracking the vegetation types corresponding to the active fires in FC_{out}, weighted by the appropriate α and γ which were unique for different aggregated vegetation classes, regions, and years.

[33] We made several small changes to the biogeochemical model compared to *van der Werf et al.* [2010]. Here we used 2001–2010 burned area observations to spin up the biogeochemical model. Also, in the original version of GFED3, burned area in forests in deforestation regions was boosted with fire persistence to gain consistency with published deforestation assessments [*PRODES*, 2012]. Here we followed the same approach and applied an additional linear scalar of 1.42 for the simulation with $BA_{MCD64A1}$ derived from a similar comparison as in *van der Werf et al.* [2010] but now with more years of deforestation data in the Brazilian Amazon from the Amazon Deforestation Monitoring Project [*PRODES*, 2012] in the optimization. For the BA_{total} run, we did not apply this scale factor to burned area in deforestation regions as deforestation rates predicted using this approach were larger than several recent estimates [*PRODES*, 2012; *Hansen et al.*, 2008]. Instead, when burned area exceeded the observed deforested area we capped the

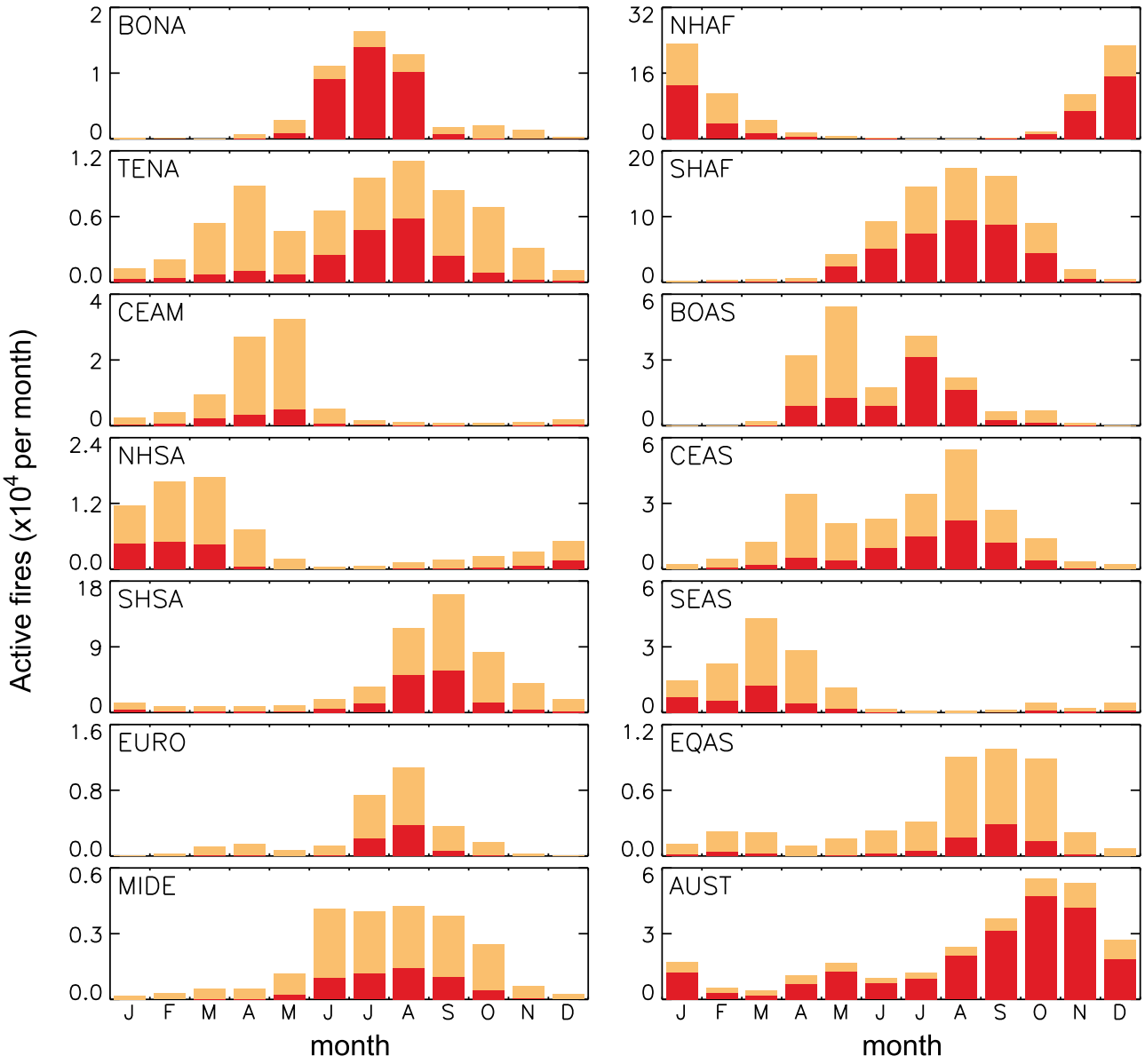

Figure 1. The number of active fires within or near burned areas (FC_{in}, red bars) or outside of burned areas (FC_{out}, light orange bars) during 2001–2010. The burned area observations used to define FC_{in} and FC_{out} are from the 500 m MCD64A1 product, and data on the active fires are from the Terra MOD14A1 product. The FC_{out} estimates are stacked on top of the FC_{in} estimates, so their sum (the height of the total bar) is equal to FC_{total}. Different continental-scale regions are abbreviated as follows: Boreal North America (BONA), Temperate North America (TENA), Central America (CEAM), Northern Hemisphere South America (NHSA), Southern Hemisphere South America (SHSA), Europe (EURO), Middle East (MIDE), Northern Hemisphere Africa (NHAF), Southern Hemisphere Africa (SHAF), Boreal Asia (BOAS), Central Asia (CEAS), Southeast Asia (SEAS), Equatorial Asia (EQAS), and Australia (AUST). A map of these regions is given in *van der Werf et al.* [2010].

burned area associated with deforestation at similar levels as in the $BA_{MCD64A1}$ run and applied this amount to the deforestation module in GFED3. The excess burned area in tropical forests was treated separately as a class of fires not directly associated with land clearing (i.e., as escaped fires or forest degradation fires).

[34] We note that even though small fires are probably less severe, as described below in Section 3 in terms of dNBR and FRP observations, this potential bias was taken into account in our emissions modeling approach because BA_{sf} was computed using γ, which in turn depends on dNBR.

3. Results

3.1. Spatial Distribution of Active Fires and Model Parameters

[35] We found good agreement between the spatial distribution of active fires and burned area in boreal forests of

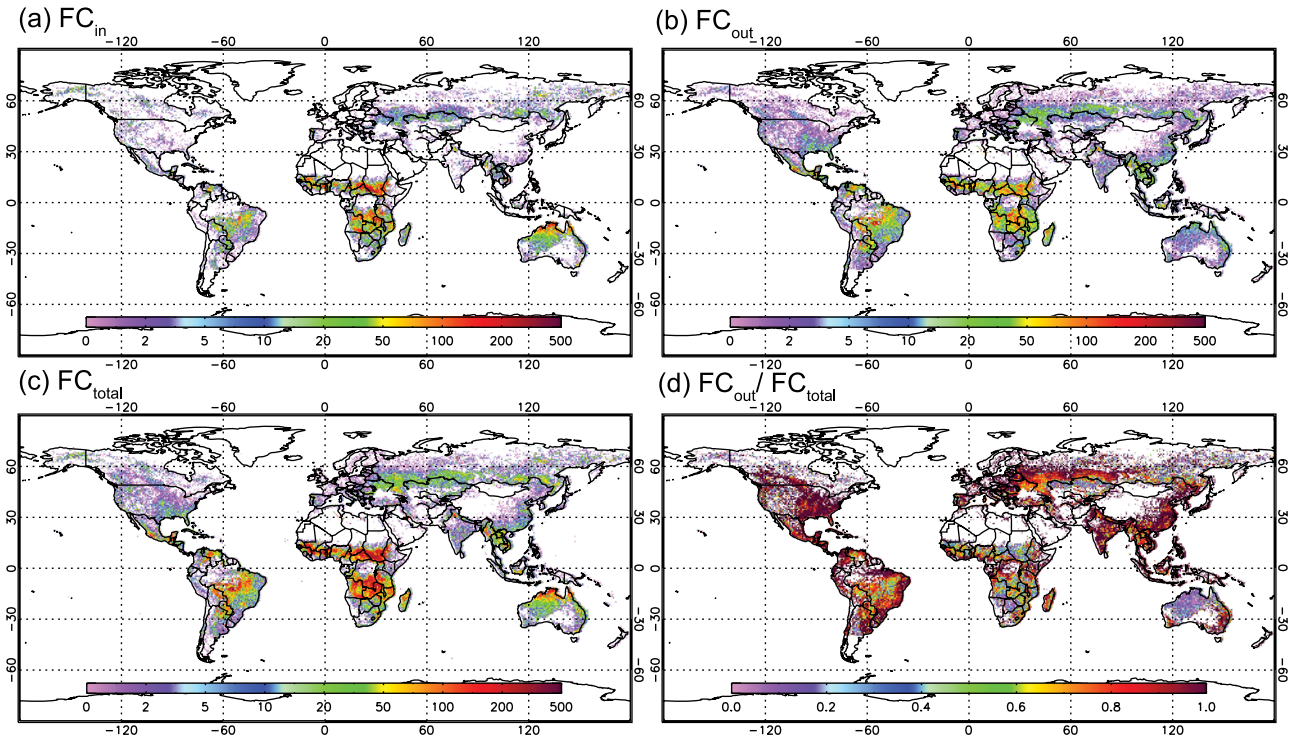

Figure 2. Annual active fire counts from MODIS Terra (number of fire counts per 0.25° grid cell per year). (a) Active fires within the perimeter of the MODIS burned area product MCD64A1 (same as FC_{in} in the text). (b) Active fires outside of MODIS burned area (same as FC_{out}). Figure 2b is the complement to FC_{in} in Figure 2a. (c) The total number of active fires in each grid cell (FC_{total}). (d) the fraction of active fires outside of burn perimeters to total active fires (FC_{out}/FC_{total}). All of the panels show annual means constructed using 2001–2010 observations.

North America and in savannas across Africa and Australia. In these regions most active fires were within or near burn scars, and so FC_{in} was larger than FC_{out} (Figures 1 and 2). In contrast FC_{out} was considerably larger than FC_{in} in temperate North America, Europe, Central America, South America, Southeast Asia, and equatorial Asia. As a function of vegetation type, on all continents FC_{out} was larger than FC_{in} in croplands and in cropland/natural vegetation mosaics. This was expected given the small field sizes and fragmented landscape that exist in many agricultural regions [*McCarty et al.*, 2009] and the challenge of detecting burn scars in areas undergoing other forms of land management such as harvesting, plowing, or irrigation. In many tropical regions FC_{out} was a larger fraction of the total number of active fires at the end of the fire season (Figure 1).

[36] α, the ratio of burned area to active fires, varied considerably as a function of vegetation type. In boreal forests, α was often less than 1 km^2/active fire, probably as a result of multiple satellite overpasses at higher latitudes each day and high fuel loads leading to multiple active fire detections for a given burned area perimeter (Figure 3). In many tropical savanna regions, in contrast, α often varied between 2 and 5 km^2/active fire, probably a result of faster moving (and short-lived) grass fires, relatively low fuel levels, and longer gaps between successive overpasses that limited the number active fires observed within burn perimeters [*Giglio et al.*, 2010].

[37] γ, the scalar adjustment to α for active fires outside of burned areas, also varied considerably as a function of region and vegetation type (Figure 3). This scalar typically varied between 0.2 and 0.6 for different seasonal periods and vegetation types, with larger values observed for Northern Hemisphere Africa, Central Asia, Southeast Asia, and smaller values in Temperate North America and Europe. Example distributions of normalized burn ratio used to derive γ for the most commonly burning aggregated vegetation class in each region, during the peak month of burning, are shown in Figure 4.

[38] In terms of spatial variability of BA_{sf} across the different continental-scale regions shown, regional differences in FC_{out} contributed to 43% of the variance, α contributed 36%, and γ contributed to 21%. Considering the full range of mean model parameters, FC_{out} varied by a factor of 26 across the different continental-scale regions, FC_{out}/FC_{total} varied by factor of 3.8, α varied by a factor of 5.0, and γ varied by a factor of 2.8.

3.2. Comparison With Regional Burned Area Products

[39] In Alaska, including small fires increased the MODIS estimates of burned area by about 8% during 2002–2010, bringing it into closer agreement with AKLFDB and MTBS products (Figure 5a). The original $BA_{MCD64A1}$ had a mean burned area of 0.65 Mha/yr during 2002–2010, approximately 24% lower than the mean from AKLFDB. The small fire algorithm (BA_{sf}) added about 0.06 Mha/yr, so that the total burned area from MODIS was 17% lower than AKLFDB. In all years, the spatial correlation coefficient between $BA_{MCD64A1}$ and AKLFDB increased by a small

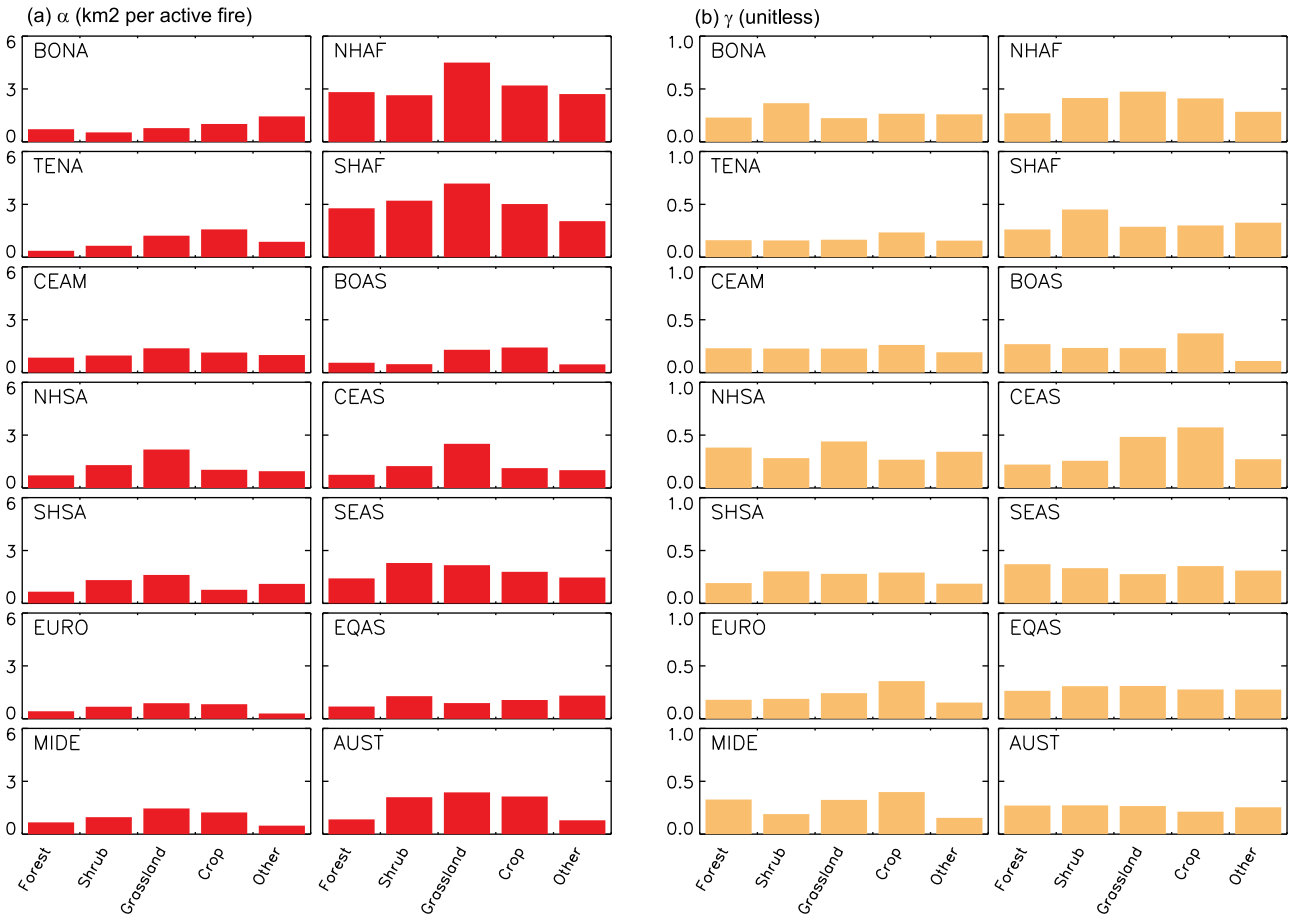

Figure 3. Model parameters α and γ for different continental-scale regions and aggregated vegetation classes averaged over 2001–2010.

amount when the small fire component was added. Averaged over each year during 2002–2010, the mean spatial correlation coefficient between $BA_{MCD64A1}$ and the AKLFDB was 0.69, and this increased to 0.71 for BA_{total}. For this same period, fires less than 1000 ha in size accounted for 1.5% of burned area in the AKLFDB. For this size class (i.e., for grid cells that had more than 50% of total burned area derived from this size class), the BA_{sf} algorithm increased MODIS burned area by 42%, whereas for grid cell dominated by large fires greater than 1000 ha, BA_{sf} increased MODIS burned area by only 8%. Further visual inspection of the spatial pattern of the FC_{out} set of active fires in Alaska showed that almost all were within or near (less than 1 km) of AKLFDB polygons, indicating that most of these pixels were associated with existing fires in the database, but in areas that may have burned only partially, as expected for example for areas near the fire perimeter or near interior unburned islands. We note that in comparisons with geographic information system polygon products, 500 m burned area products such as MCD64A1 are expected to yield lower estimates because small unburned islands will be excluded from this product when the algorithm is applied on a pixel by pixel basis. For example, using a dNBR-based classification tailored specifically for fires in Alaska, *Beck et al.* [2011] estimated that unburned islands accounted 3% of the interior area of low severity polygons and 7% for high severity polygons.

[40] In Canada, the CNFDB was higher than the original $BA_{MCD64A1}$ in all years. The small fire algorithm increased the MODIS mean during 2002–2010 (Figure 5b) and slightly increased the spatial correlation in all but one of these years in non-agricultural areas. BA_{sf} considerably modified MODIS burned area estimates across the wheat belt in Saskatchewan and across the southwestern parts of British Columbia and Alberta (Figure S2 in the auxiliary material). Burned area more than tripled in agricultural areas, from 0.04 to 0.14 Mha/yr, when small fires were included. In Canada, fires less than 1000 ha in size accounted for 4.1% of burned area in the point version of the CNFDB. For this size class, the BA_{sf} algorithm increased MODIS burned area by 98%, whereas for larger fires greater than 1000 ha, BA_{sf} increased MODIS burned area by only 4%.

[41] In the continental U.S. the small fire algorithm increased the total amount of MODIS burned area considerably, by approximately 75% during 2001–2010 (Table 1), and brought the MODIS-based estimates into closer agreement with several estimates. For areas that experienced large wildland fires, defined as 0.25° grid cells that had at least 1 fire during 2002–2010 in the MTBS database, the small fire algorithm increased MODIS burned area by 16% (Figure 5c). $BA_{MCD64A1}$ was 60% of the MTBS mean during 2002–2010, and this percentage increased to 70% for BA_{total}. For the

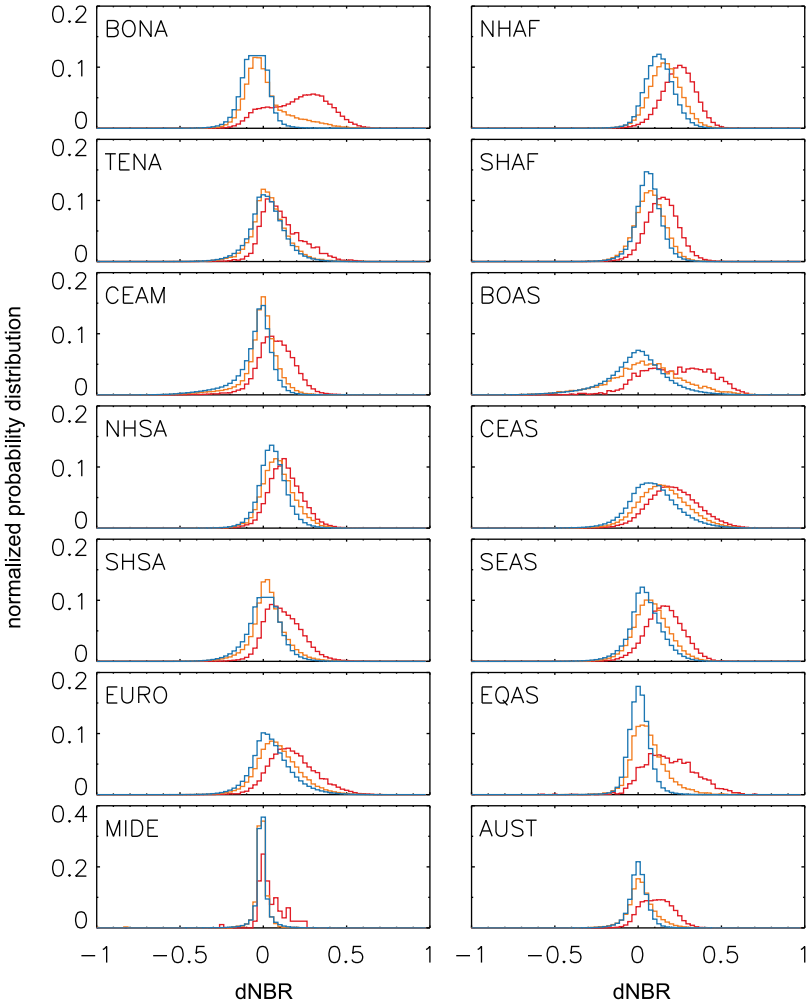

Figure 4. The distribution of difference normalized burn ratio (dNBR) for active fires within burned areas from MCD64A1 (red), outside of burned areas (orange) and for control areas (blue). The distributions were constructed during the peak fire month using the most commonly burning vegetation type with each region. The distributions were generated using observations made between 2001 and 2010.

MTBS data set, fires less than 1000 ha in size accounted for 12% of the total burned area. For this size class, the BA_{sf} algorithm increased MODIS burned area by 70%, whereas for larger fires greater than 1000 ha, BA_{sf} increased MODIS burned area by only 12%.

[42] Both of the MODIS estimates were broadly consistent with MTBS burned area given, for example, that 28% of the area within MTBS polygon perimeters was classified as "unburned to low severity" for the Pacific Northwest and Pacific Southwest during 1984–2005 [*Schwind et al.*, 2008]. It was not possible to further quantify if BA_{sf} improved MODIS estimates for MTBS because statistics on unburned islands were not readily available for the continental-scale MTBS polygon data set, and because it was not possible to simulate the "unburned to low severity" MTBS class with our $BA_{MCD64A1}$ and BA_{sf} algorithms, given that these classes were computed from different temporal intervals of dNBR for each fire in the MTBS database. Also, it is likely that some fires not digitized as a part of the MTBS project were included in some of the overlapping 0.25° grid cells for BA_{total}.

[43] For croplands in CONUS, including small fires improved comparisons with published estimates for this biome. The original $BA_{MCD64A1}$ had a 2003–2007 mean of 0.26 ± 0.06 Mha/yr for U.S. croplands, defined by burned area in cropland and cropland and natural vegetation mosaic 500 m pixels using the IGBP classification from *Friedl et al.* [2010]. The small fire algorithm tripled this estimate, yielding a total burned area mean of 0.85 ± 0.08 Mha/yr and bringing our estimates into closer agreement with previous estimates for this biome of 1.24 ± 0.07 Mha/yr from *McCarty et al.* [2009] for this same period (Figure 5d).

[44] After removing the wildland fire and agricultural burned area components described above from $BA_{MCD64A1}$ and BA_{total}, we obtained residuals for CONUS of 0.22 ± 0.06 Mha/yr Mha/yr and 0.69 ± 0.28 Mha/yr during 2002–2010. Comparing these residuals to the NIFC reports of prescribed fires for this period (1.03 ± 0.15 Mha/yr), small fire burned area considerably improved the magnitude of the agreement though BA_{total} remained below NIFC prescribed fire reports for most years (Figure 5e). The spatial distribution of this residual burned area for BA_{total} was concentrated

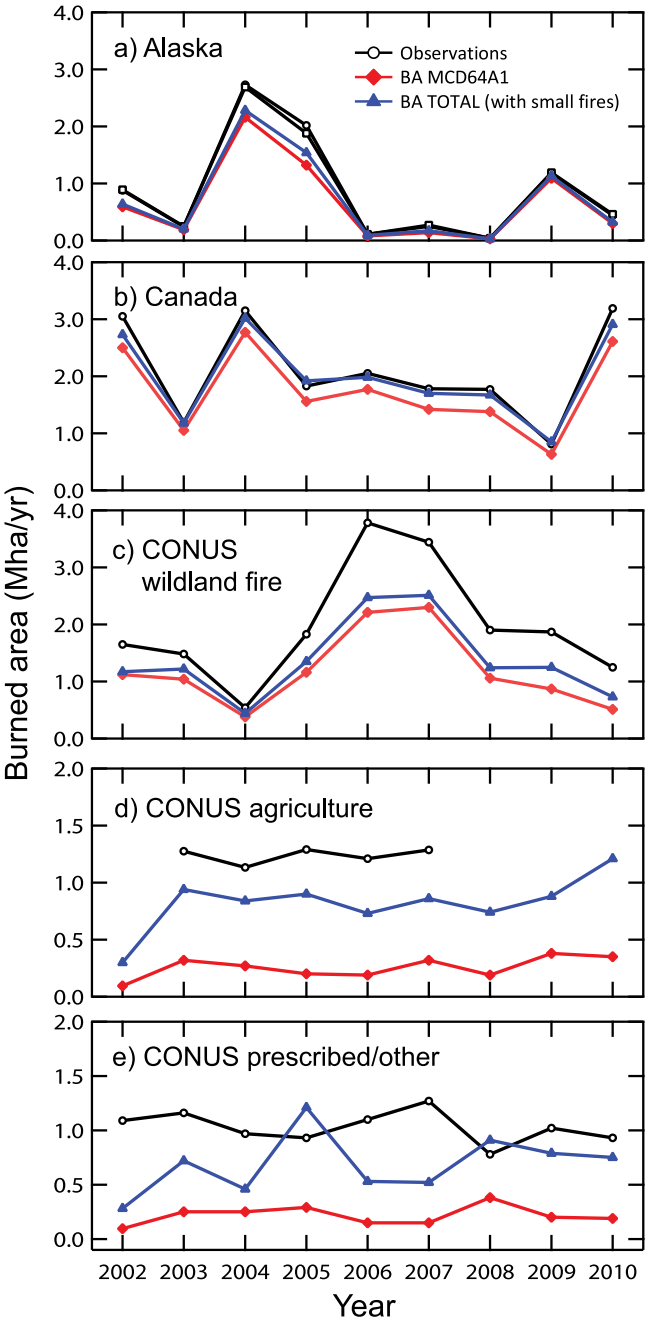

Figure 5. Comparison of MODIS burned area products with regional burned area products for North America. The regional observations are shown in black, the MODIS MCD64A1 burned area is shown in red, and MODIS total burned area, including the small fire burned area developed here, is shown in blue. In Figure 5a, observations for Alaska are provided from both the Alaska Large Fire Database (AKLFDB, black squares) and the Monitoring Trends in Burn Severity (MTBS) project (black circles).

in the Southeast (Figure 6), which is consistent with extensive use of prescribed burning for forest and plantation management in this region. Small fires modestly improved the spatial agreement across the 48 states between the NIFC prescribed fire estimates and the MODIS residual, with the correlation coefficient for the 2002–2010 mean increasing from 0.28 for $BA_{MCD64A1}$ to 0.30 for BA_{total}.

[45] For Portugal, for the entire domain of the country the two MODIS burned area estimates were lower than the national polygon data set during 2002–2009, by 24% for $BA_{MCD64A1}$ and 7% for BA_{total} (Figure S3 in the auxiliary material). In 7 of 8 years, BA_{total} had a higher spatial correlation with the national data set than $BA_{MCD64A1}$, and over the full period small fires increased the spatial correlation coefficient on average from 0.67 to 0.70 (Figures S4 and S5 in the auxiliary material).

[46] For the savanna ecosystem region in Mali studied by *Laris* [2005], including small fires increased MODIS burned area during the 2002–2003 fire season from 24% to 33% of the study area. Compared to the Landsat-derived estimate of 57% for this domain [*Laris*, 2005], accounting for small fires improved the agreement but did not eliminate the low biases observed for the MODIS burned area product. The relative monthly increases from including small fires were largest at the beginning and end of the fire season, when the prevalence of small and fragmented burns was higher based on the Landsat-derived perimeter to burned area ratios (Table 2).

3.3. Impacts of Small Fires on Global and Regional Burned Area Patterns

[47] At a global scale, including small fires increased burned area by 35% or 120 Mha/yr during 2001–2010 (Table 1). Most of the global increase was driven by small fires in Southern Hemisphere Africa (42.3 Mha/yr), Northern Hemisphere Africa (36.0 Mha/yr), Southern Hemisphere South America (10.2 Mha/yr), Central Asia (10.1 Mha/yr), and Southeast Asia (6.0 Mha/yr). In terms of relative changes, Equatorial Asia had the largest increase (157%), followed by Central America (143%), Europe (112%), Southeast Asia (90%), and the Middle East (90%). As a function of vegetation type, woody savannas (46.4 Mha/yr), savannas (30.5 Mha/yr), croplands (11.8 Mha/yr), cropland and natural vegetation mosaics (11.2 Mha/yr), and grasslands (9.6 Mha/yr) accounted for most of the increase in burned area (Table 3). Averaged over the decade we estimated about 464 Mha, or 3.5% of the ice-free land surface, burned each year.

[48] At a regional scale, large relative increases in burned area occurred across eastern North America, southern Mexico, Central America, Eastern Europe, Central Asia, and many countries in Southeast Asia (Figures 7 and 8). Many of these increases were driven by a much higher detection efficacy of the small fire burned area algorithm in croplands, cropland and natural vegetation mosaics, and evergreen broadleaf forests (Table 3). From an emissions perspective, the increase of 119% of burned area in evergreen broadleaf forests is particularly important because of the high fuel loads present in this biome. Equatorial Asia had one of the largest relative increases in burned area of any region (157%). The small fire burned area product in this region revealed a much more extensive distribution of burning across Sumatra and in western and interior areas of Borneo (Figure 8). Although the amount of burned area in equatorial Asia is quite low compared to Africa and other regions, many of these fires occur in fuel-rich tropical peatlands [*Page et al.*, 2002] that have a high sensitivity to ENSO-induced variability in regional climate [*Field et al.*, 2009; *Tosca et al.*, 2011].

Table 1. Burned Areas by Region Averaged During 2001–2010

Region[a]	Original MODIS 500 m Burned Area ($BA_{MCD64A1}$; Mha/yr)	Burned Area From Small Fires (BA_{sf}; Mha/yr)	Total Burned Area (BA_{total}; Mha/yr)	Increase From BA_{sf} (%)	CV[b] for $BA_{MCD64A1}$	CV for BA_{sf}	CV for BA_{total}
BONA	2.3	0.3	2.6	14	0.56	0.35	0.50
TENA	1.6	1.2	2.7	75	0.41	0.35	0.30
CEAM	1.4	2.0	3.4	143	0.51	0.23	0.30
NHSA	2.9	2.3	5.1	79	0.22	0.18	0.19
SHSA	18.5	10.2	28.7	55	0.47	0.20	0.36
EURO	0.5	0.6	1.1	112	0.42	0.33	0.31
MIDE	0.7	0.6	1.2	90	0.40	0.37	0.38
NHAF	117.9	36.0	154.0	31	0.10	0.11	0.10
SHAF	126.2	42.3	168.5	34	0.07	0.05	0.05
BOAS	6.0	3.8	9.8	62	0.76	0.47	0.59
CEAS	14.1	10.1	24.2	72	0.31	0.17	0.22
SEAS	6.7	6.0	12.6	90	0.37	0.28	0.30
EQAS	0.7	1.1	1.8	157	0.82	0.42	0.52
AUST	45.2	3.3	48.5	7	0.49	0.42	0.49
Global:	344.6	119.7	464.3	35	0.07	0.04	0.06

[a]The different regions are defined in the caption for Figure 1.
[b]CV is the coefficient of variation computed over the 2001–2010 period using the annual mean observations from each year. CV is defined as the standard deviation divided by the mean.

3.4. Small Fires Effects on Seasonal and Interannual Variability of Burned Area

[49] In tropical forest and savanna regions, including small fires modified the annual cycle of burned area by extending the fire season. Specifically, small fires increased burned area by a larger amount at the end of the fire season than at the beginning of the fire season (Figure 9). This effect was most pronounced in Central America, Equatorial Asia, Southeast Asia, and South America. The greater contribution from active fire detections to BA_{total} in the late dry season may also reflect difficulties with burned area mapping during the dry-wet transition due to higher cloud cover or aerosol concentrations. In Central and Boreal Asia, in contrast, small fires had the largest impact on total burned area during spring, at the onset of the fire season. These changes in the annual cycle were mostly driven by patterns of FC_{out} and are visible in the ratio of FC_{out} to FC_{total} shown in Figure 1. Seasonal changes in α and γ appeared to have only

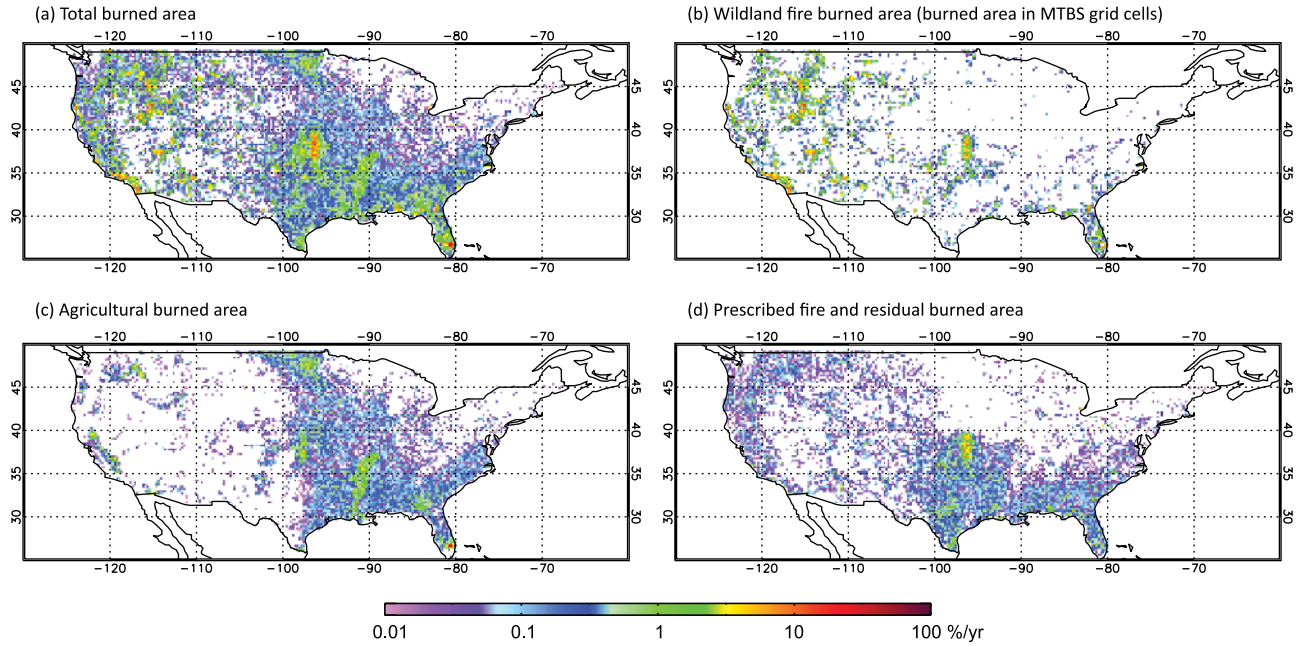

Figure 6. MODIS burned area fraction for the continental U.S. (BA_{total}) for (a) all fires, (b) burned area annually coincident at a 0.25° spatial resolution with Monitoring Trends in Burn Severity (MTBS) project fire scars, (c) agricultural fires, and (d) prescribed/other fires. Figure 6c was constructed by sampling BA_{total} in areas where 500 m vegetation cover maps indicated either croplands or croplands and natural vegetation mosaics. Figure 6d was constructed by subtracting fires shown in Figures 6b and 6c from those shown in Figure 6a. This residual includes prescribed fires and other fires that were not associated with MTBS perimeters or cropland areas.

Table 2. MODIS Burned Area Comparisons With Landsat-Derived Estimates From *Laris* [2005]

	MODIS-Derived Burned Area			Burned Area Estimates for Southern Mali, Africa [From *Laris*, 2005]	
Time Period	$BA_{MCD64A1}$ (% of Study Area per Month or Year)	BA_{total} (% of Study Area per Month or Year)	Increase From Small Fires (%)	Landsat-Derived Burned Area (% of Study Area per Month or Year)	Landsat-Derived Perimeter of Burned Area Ratio
September–November 2002	1.1	4.9	345	17.6	0.305
December 2002	14.3	17.9	25	23.9	0.235
January 2002	6.6	7.5	14	10.5	0.217
February 2002	2.0	2.6	30	4.9	0.429
Total 2002–2003 fire season	24.0	32.9	37	56.9	

a secondary effect on the annual cycle of small fire burned area, and also on patterns of interannual variability.

[50] One possible mechanism for the larger relative contribution of small fires to total burned area at the beginning and end of the fire season is that fires during these periods are more fragmented as a consequence of higher vegetation and soil moisture levels. During these times, patches of the landscape may have fuel moisture levels that are too high to burn, limiting the spread of large fires. This hypothesis is consistent with the mechanisms proposed by *Laris* [2005] to describe the seasonal dynamics of fires in wooded savanna ecosystems in Mali. Fire perimeter to burned area ratio observations from *Laris* [2005] indicate that larger fires occur in the middle of the fire season, when fuel moisture levels are sufficiently low to allow combustion in all vegetation types present in landscape mosaics (Table 2).

[51] From year to year, small fire burned area was considerably less variable than MCD64A1 burned area in many regions, including Central America, Southern Hemisphere South America, Southeast Asia, and Central Asia (Figure 10 and Table 1). Globally, the coefficient of variation for BA_{sf} was approximately 40% lower than that for $BA_{MCD64A1}$ (Table 1). One hypothesis for the less variable BA_{sf} is that these fires are more closely linked with different forms of land management, such as agricultural waste burning or prescribed burning in forest plantations. Specifically, incentives may exist for land managers not to allow these fires burn out of control and damage nearby areas. If and when these fires do escape control, it may be as a consequence of anomalously dry climate conditions, leading to larger and more severe fires, and ones that would be more easily detected by the $BA_{MCD64A1}$ product.

3.5. Sensitivity Test Results

[52] Mean fire radiative power for individual fire detections was lower on average for active fires outside of MCD64A1 burned area than for active fires within the perimeter of these burn scars (Table 4). This is consistent with the premise that active fires associated with FC_{out} were often smaller and thus more difficult to detect using burned area algorithms applied to moderate resolution surface reflectance time series. In many regions, the cumulative fire radiative power outside of burned areas, defined as the mean fire radiative power per active fire detection multiplied by the total number of active fires in this set during the time of the Terra overpass, was considerably larger than the cumulative fire radiative power within burned areas.

[53] Sensitivity simulations for the year 2010 provided some information about the likely uncertainty in our estimates of burned area associated with small fires. Using active fires from Aqua increased our small fire burned area estimates by approximately 49% at a global scale. Two thirds of this increase was driven by a greater fraction of active fires occurring outside of burned areas during Aqua overpasses than during Terra overpasses. A likely explanation for this is that the diurnal cycle for smaller fires has a stronger peak in mid-day and thus proportionally more are detected during the nominal 1:30 pm overpass for Aqua. This finding is also consistent with diurnal cycles derived for different vegetation types from GOES that show more pronounced diurnal cycles in agricultural regions and tropical

Table 3. Burned Area by Vegetation Type Averaged During 2001–2010

Vegetation Type	Original MODIS 500 m Burned Area ($BA_{MCD64A1}$; Mha/Year)	Burned Area From Small Fires (BA_{sf}; Mha/Year)	Total Burned Area (BA_{total}; Mha/Year)	Increase From Small Fires (%)
Evergreen Needleleaf Forests	1.7	0.3	2.0	17
Evergreen Broadleaf Forests	3.1	3.6	6.7	119
Deciduous Needleleaf Forests	1.1	0.2	1.3	22
Deciduous Broadleaf Forests	3.4	1.3	4.7	39
Mixed Forests	1.1	0.8	1.9	75
Closed shublands	2.1	0.7	2.8	33
Open shrublands	17.9	1.7	20.0	10
Woody Savannas	136.2	46.4	182.6	34
Savannas	114.3	30.5	144.8	27
Grasslands	38.5	9.6	48.1	25
Permanent Wetlands	1.2	0.8	2.0	67
Croplands	9.6	11.8	21.4	123
Urban	0.1	0.5	0.5	834
Croplands and Natural Vegetation Mosaics	14.3	11.2	25.5	79
Barren	0.2	0.1	0.3	71

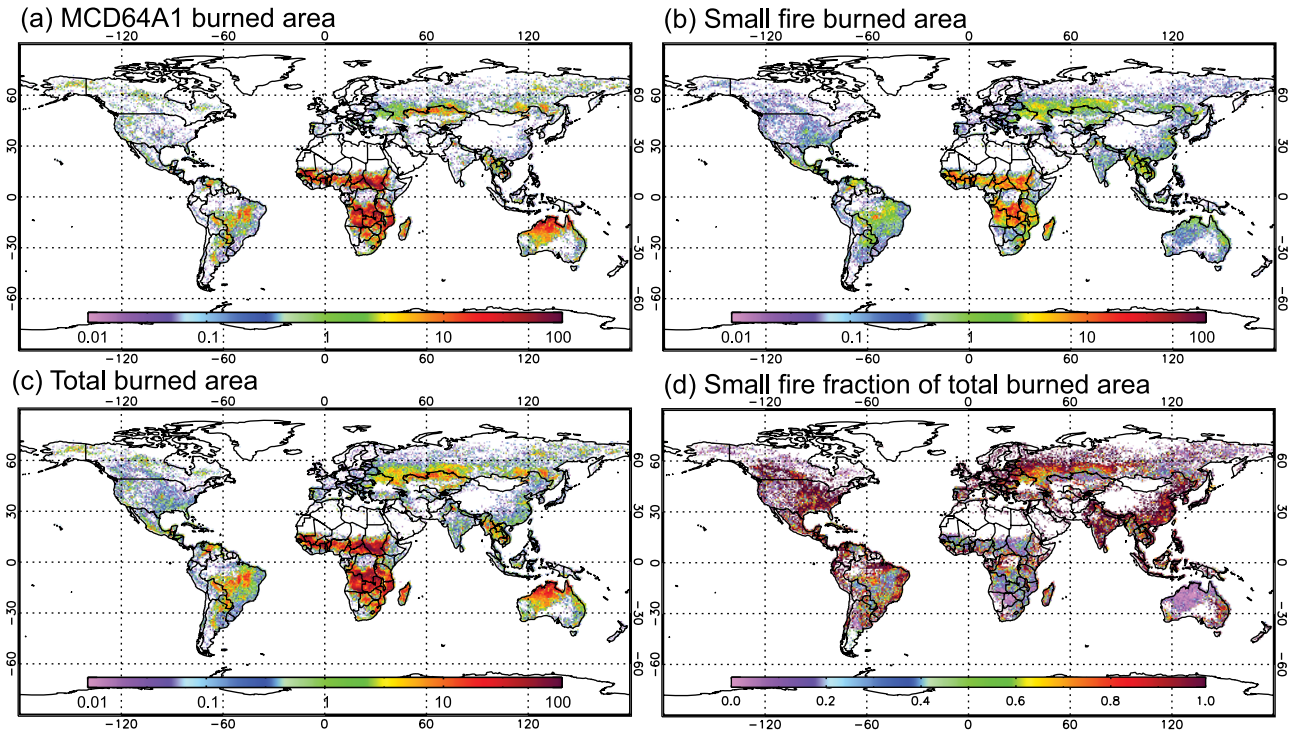

Figure 7. Percentage per year of burned area fraction in each 0.25° grid cell associated with (a) the original 500 m MODIS burned area product ($BA_{MCD64A1}$), (b) the small fire burned area product developed here (BA_{sf}), and (c) the total MODIS burned area (BA_{total}). (d) The ratio of small fire to total burned area in each grid cell (BA_{sf}/BA_{total}). These panels show the annual mean burned area fractions averaged using all available data during 2001–2010.

forest ecosystems than for fires occurring in temperate and boreal shrublands and forests [*Mu et al.*, 2011]. The inferred values of γ also increased, suggesting the size of individual fire scars for FC_{out} derived from Aqua also increased.

[54] Sampling burn perimeters in the exact same location but in the year before burning as a dNBR control in equation (4) reduced our estimates of small fires by approximately 15% globally. Similarly, using 8-day surface reflectance (MOD09A1) instead of the 16-day vegetation index product (MOD13A1) to derived dNBR reduced our estimates by 16% globally. One possible issue related to use of the 8-day surface reflectance is the presence of residual cloud contamination [*Loboda et al.*, 2007] that may be minimized with the compositing and longer sampling interval of the MOD13A1 product. Using only middle and high confidence active fire retrievals from Terra for the computation of α and γ had only a minor effect on our results, increasing small fire burned area by 6%. Within individual regions, the impact of changing these model parameters varied considerably (Table S1 in the auxiliary material). An important next analysis step is to assess how the different assumptions examined in the sensitivity analysis impact the comparisons with evaluation data sets from the Canada, the United States, Portugal, and Mali. This may guide future refinements to estimates of small fire burned area. A summary of the sensitivity results and their impact on BA_{total} for different regions (and globally) is shown in Table S1.

[55] Among the different combinations of sensitivity tests, using middle and high confidence active fires and observations from Aqua would lead to a 55% increase in global BA_{sf} (assuming the changes from these two tests are additive) whereas using Terra active fires with 8-day surface reflectance and an alternative approach for constructing the pre-fire dNBR control would lead to a 31% decrease. This −31 to +55% range across all the tests provided some information about uncertainty levels. More formal estimates of uncertainties (i.e., 95% confidence limits) were not possible at this stage for BA_{sf} because of a lack of quantitative information regarding uncertainties in the different satellite products we used and also because of a paucity of high resolution burned area observations required for validation. Approaches for quantifying and reducing uncertainties in future work are discussed in Section 4.

3.6. Effects of Small Fires on Biomass Burning Carbon Emissions

[56] Global carbon emissions during 2001–2010 increased by 35%, from 1.9 Pg C/yr to 2.5 Pg C/yr, when BA_{sf} was included in GFED3 simulations (Figure 11 and Table 5). Within most regions, the relative increase in emissions from including small fires was smaller than that for burned area, as a consequence of more BA_{sf} occurring in vegetation types with lower fuel loads (e.g., agriculture) and during times when climate and fire persistence controls on combustion completeness caused lower levels of fuel consumption within the model. One exception to this was Central Asia where small fire burned area increased carbon emissions from vegetation types with higher fuel loads. Even though 13 of 14 regions had relative increases in emissions that were smaller than the relative increases in burned area, globally the percent increase in emissions (35%) was the

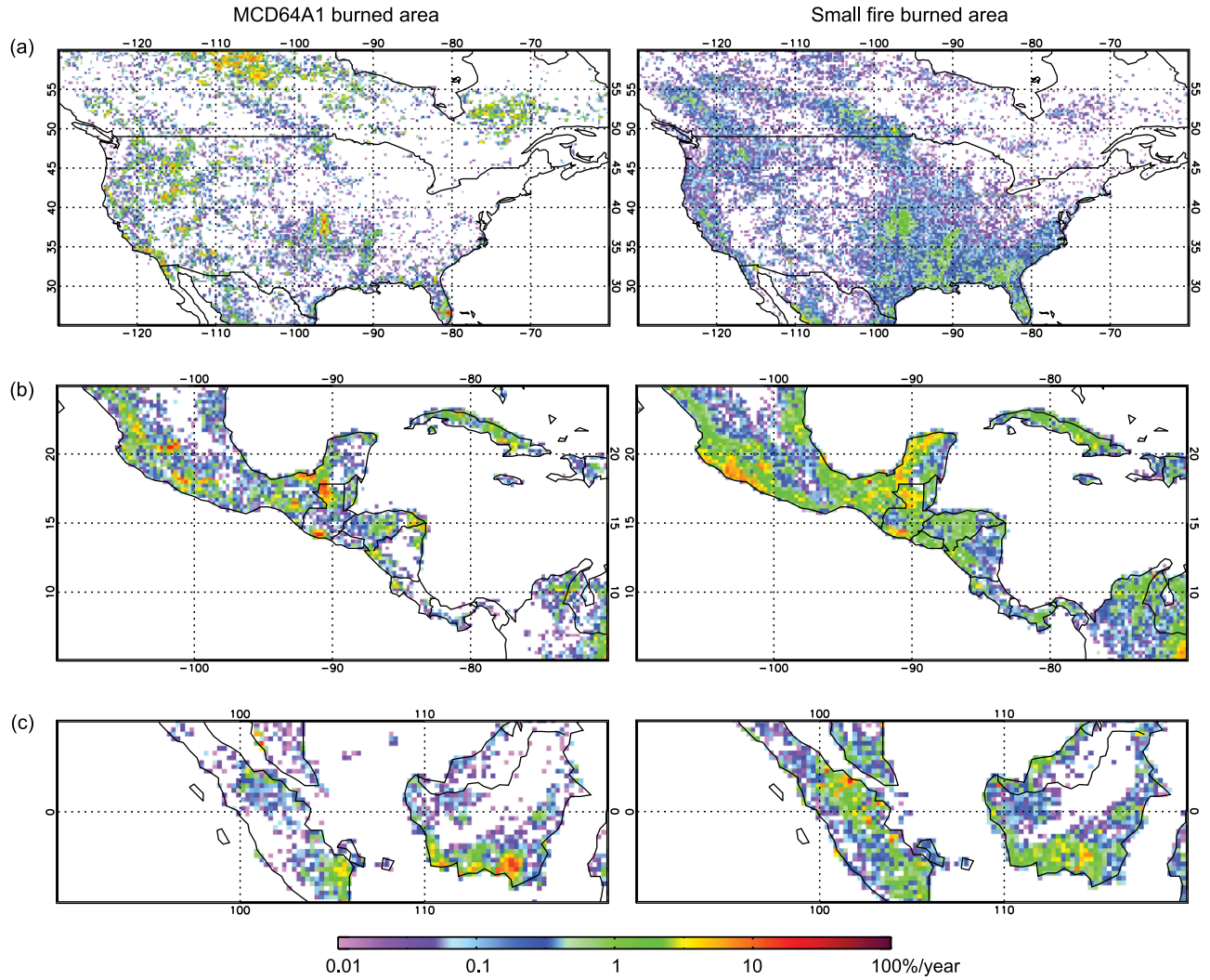

Figure 8. (left) The MODIS burned area product ($BA_{MCD64A1}$) and (right) the small fire product developed here (BA_{sf}) for temperate North America, Central America, and Indonesia. Units are percentage of each 0.25° grid cell per year averaged over 2001–2010.

same as for burned area. This was possible because large contributions to the total carbon emissions from BA_{sf} originated from regions with low levels of burned area, but high levels of mean annual emissions. Specifically, Central America, Northern Hemisphere South America, Southern Hemisphere South America, Southeast Asia, and Equatorial Asia accounted for over 42% of the carbon flux derived from small fires, yet only 18% of BA_{sf}. The standard deviation of annual mean carbon emissions from these regions during 2001–2010 increased as a consequence of small fires increasing burned area by a considerable amount in tropical forest areas. In other regions, with the exception of Northern Hemisphere Africa, the standard deviation of annual carbon emissions also increased during 2001–2010, though by a smaller amount.

4. Discussion

4.1. Overview

[57] The difficulty of detecting small fires with moderate resolution surface reflectance imagery has been noted in many studies [*Eva and Lambin*, 1998; *Simon et al.*, 2004; *Hoelzemann et al.*, 2004; *Laris*, 2005; *Roy and Landmann*, 2005; *Silva et al.*, 2005; *Loboda et al.*, 2007; *McCarty et al.*, 2009; *Roy and Boschetti*, 2009]. Burned area detection algorithms have to distinguish fires from many other forms of land cover change, including seasonal changes in leaf area and leaf senescence, synoptic and seasonal changes in soil moisture, and other forms of disturbance such as harvesting, plowing, insect outbreaks, and hurricanes. This classification problem places stringent requirements on the thresholds for change detection. As a consequence, a substantial fraction of a pixel must be completely burned to avoid serious commission errors that would degrade the usefulness of a regional or global burned area product derived using moderate resolution surface reflectance imagery. Indeed, many developers of global burned area products have opted to accept larger omission errors than commission errors in their algorithm design [*Roy and Boschetti*, 2009]. We argue that while it will be possible to refine burned area detection algorithms in future work, the intrinsic tradeoff between commission errors and threshold

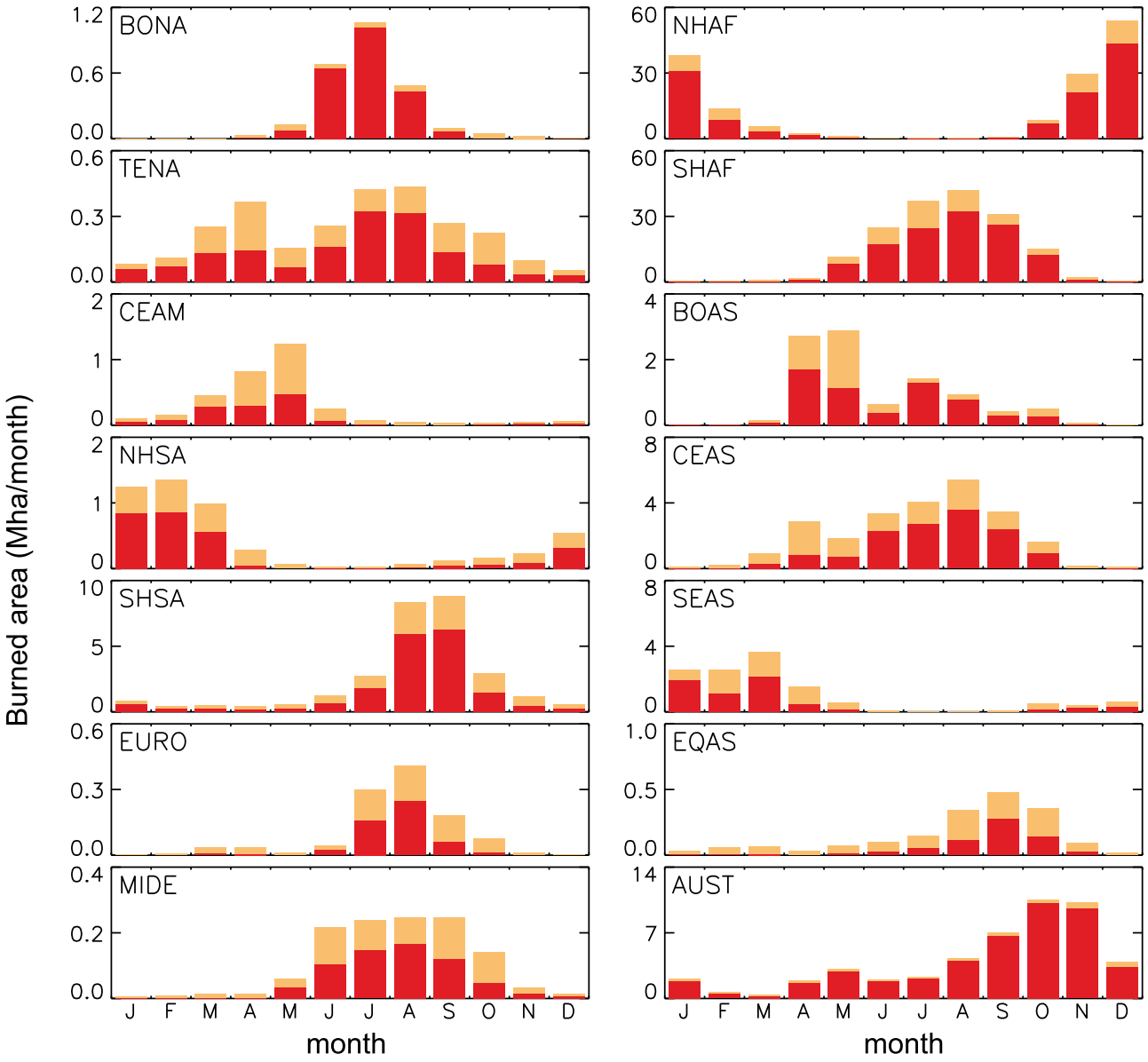

Figure 9. Seasonal dynamics of burned area for different continental scale regions (with units of Mha per month) for the original 500 m MODIS burned area product ($BA_{MCD64A1}$) denoted by red bars and the additional small fire burned area product developed here (BA_{sf}) denoted by orange bars. These panels show the annual mean burned area averaged during 2001–2010.

relaxation may make it impossible for these algorithms to work effectively for some sub-pixel burns. Instead, other approaches are needed to quantify burned area and emissions for this class of fires.

[58] Here we developed an approach for quantifying these fires consisting of two stages: (1) we computed number of active fires inside and outside of burned areas (FC_{in} and FC_{out}) to identify the relative contribution and spatial location of small fires, and (2) we computed dNBR changes separately for FC_{in} and FC_{out} to estimate BA_{sf}. With this method, we avoided having to design a detection algorithm that separated small fires from all other sources of surface reflectance variation. In effect, we were able to draw upon the skill of the MCD64A1 burned area product in classifying large fires to simplify our analytical approach. Other approaches may be possible, including for example empirically relating FC_{out} to high spatial resolution burned area observations, modeling burned area–fire size relationships using a combination of higher resolution Landsat imagery and coarser resolution burned area and land cover products, or by using fire radiative power. As discussed below, however, further reductions in uncertainty using any of these methods will be limited without new approaches for validation that specifically target regions where small fires are common.

[59] Our study provides evidence that fires below the detection limit for MODIS MCD64A1 burned area can have important consequences for burned area and biomass burning emissions. In North America, Portugal, and parts of Mali, by accounting for these fires, we improved the agreement between MODIS burned area and several aspects of

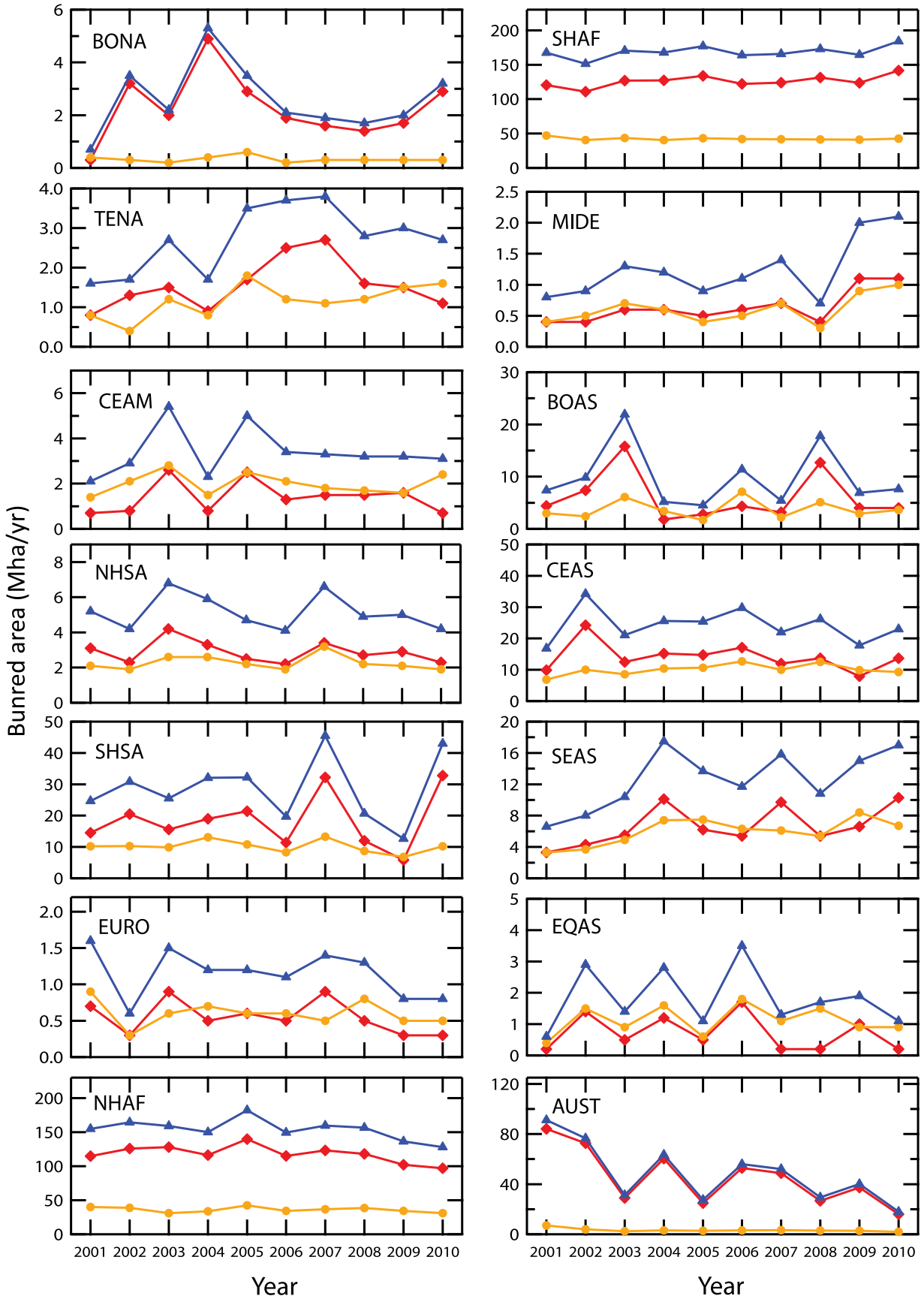

Figure 10. Burned area time series during 2001–2010 for $BA_{MCD64A1}$ (red diamonds), BA_{sf} (orange circles), and the combined total (blue triangles). The unit of measure is Mha/yr.

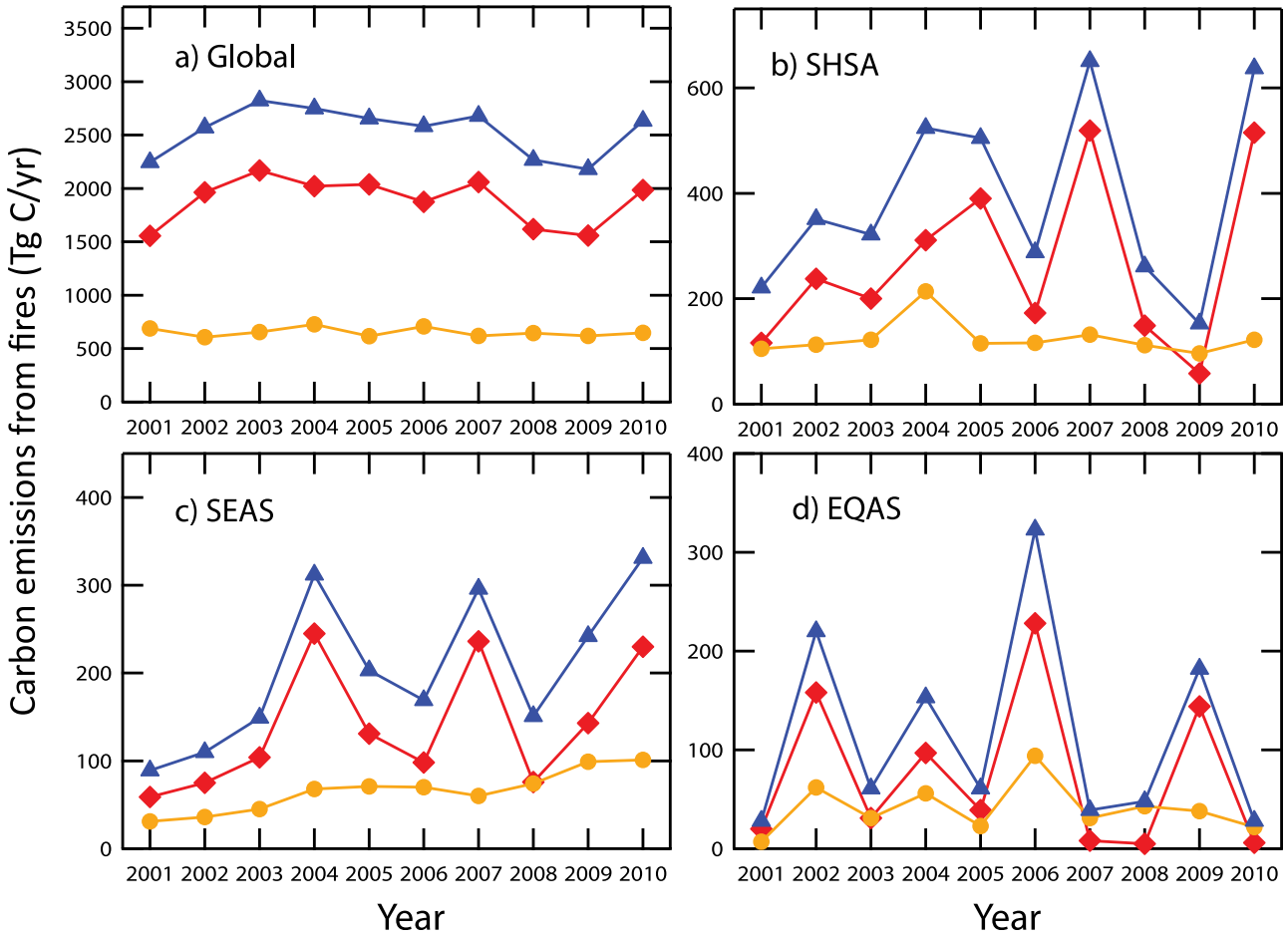

Figure 11. Carbon emissions from fires time series during 2001–2010 for GFED3 simulations driven by $BA_{MCD64A1}$ (red diamonds), BA_{sf} (orange circles), and the combined total (blue triangles). The units are Tg C/yr. The regions are (a) global and (b) Southern Hemisphere South America, Southeast Asia, and Equatorial Asia.

these regional burned area data sets. Specifically, for boreal forest fires in Alaska and Canada, our algorithm reduced the low bias observed in past work for MODIS burned area products [*Kasischke et al.*, 2011] and slightly improved correlations describing the spatial pattern of burned area each year. For the continental U.S., significant improvements were observed for agricultural and prescribed fire burned area comparisons. In Portugal, the spatial correlation

Table 4. Fire Radiative Power and Active Fires Within and Outside of MODIS Burned Areas

Region	Mean FRP for FC_{in} (MW)	Mean FRP for FC_{out} (MW)	Ratio (FRP_{out}/FRP_{in})	FC_{in} ($\times 10^4$/Year)	FC_{out} ($\times 10^4$/Year)	FC_{out}/FC_{total}	Cumulative FRP_{in} ($\times 10^4$ MW/Year)	Cumulative FRP_{out} ($\times 10^4$ MW/Year)	Ratio (Cum. FRP_{out}/ Cum. FRP_{in})
BONA	50	33	0.65	3.5	1.4	0.29	176	47	0.26
TENA	48	18	0.37	2.0	5.0	0.71	97	86	0.89
CEAM	17	12	0.73	1.4	7.4	0.84	23	92	3.97
NHSA	16	11	0.71	1.8	5.0	0.74	28	56	1.99
SHSA	24	15	0.65	15.7	36.1	0.70	371	557	1.50
EURO	28	13	0.45	0.7	2.2	0.75	20	28	1.38
MIDE	20	12	0.62	0.5	1.7	0.75	11	20	1.87
NHAF	18	11	0.64	42.5	34.3	0.45	750	386	0.51
SHAF	20	12	0.62	38.8	35.5	0.48	755	431	0.57
BOAS	29	19	0.66	8.3	9.9	0.54	242	189	0.78
CEAS	28	14	0.52	7.6	15.6	0.67	212	226	1.07
SEAS	14	12	0.90	3.3	9.8	0.75	46	120	2.63
EQAS	16	13	0.81	0.8	3.6	0.82	12	46	3.73
AUST	29	18	0.61	21.1	5.9	0.22	615	105	0.17
Global	23	14	0.61	148.1	173.4	0.54	3357	2388	0.71

Table 5. Fire Carbon Emissions by Region Averaged During 2001–2010

Region	C Emissions From $BA_{MCD64A1}$[a] (Tg C/yr)	C Emissions From BA_{sf} (Tg C/yr)	C Emissions From BA_{total} (Tg C/yr)	Increase From Small Fire Emissions (%)
BONA	58	5	63	9
TENA	10	8	18	81
CEAM	24	24	48	101
NHSA	28	20	49	72
SHSA	267	125	391	47
EURO	3	3	7	98
MIDE	1	1	3	90
NHAF	461	124	585	27
SHAF	555	154	709	28
BOAS	107	38	145	35
CEAS	32	35	67	107
SEAS	140	66	205	47
EQAS	74	41	114	55
AUST	122	10	132	9
Global	1884	654	2538	35

[a]The carbon emissions for the baseline run ($BA_{MCD64A1}$) were about 2% lower than the original GFED3 estimates from *van der Werf et al.* [2010] at a global scale, although regional differences were larger and followed variations in burned area.

between MODIS burned area and the national estimates increased in 7 of 8 years. In Mali, our small fire algorithm improved the agreement with Landsat-derived observations, with the largest relative adjustments occurring at the beginning and end of the fire season. More validation is needed, and observed differences between the spatial distribution of active fires and burned area may allow for the identification of regions for more intensive study.

[60] The increases in carbon emissions associated with small fires may have implications for several carbon cycle, atmospheric chemistry, and human health issues. Higher levels of emissions are likely to reduce low biases in carbon monoxide and aerosols observed in atmospheric models driven by earlier versions of satellite-based fire emissions inventories [e.g., *Tosca et al.*, 2012]. Also, fire contributions to variability in atmospheric CO_2 and CH_4 [e.g., *Prentice et al.*, 2011] will likely increase when small fires are accurately classified and represented in biogeochemical models. Evidence for this comes from our GFED3 simulations that showed that the standard deviation of annual mean emissions increased in all regions except Northern Hemisphere Africa during 2001–2010 when we included BA_{sf} in our simulations. In the tropics, the response of fire emissions to El Nino/Southern Oscillation, the Atlantic Multidecadal Oscillation, and other climate modes [e.g., *Chen et al.*, 2011] is likely to be higher when small fires are integrated into emissions inventories because of the large relative increases in burned area in drought-sensitive forests and peatlands across South America and Southeast Asia (Table 3 and Figure 8).

[61] Across different continents, carbon emissions increases from small fires were higher in more densely populated areas. As a result, episodic and chronic exposure to fire-emitted particulate matter and ozone, and thus fire-induced human mortality [*Johnston et al.*, 2012], is likely to be considerably higher than for estimates derived from GFED3. An important next step in this context is to more systematically quantify small fire impacts on atmospheric composition and exposure using a chemical transport model. Another critical issue is to assess overlap with inventories that include open field agricultural waste burning [e.g., *Yevich and Logan*, 2003].

4.2. Applicability to Other Burned Area Mapping Efforts

[62] Do our results have applicability for moderate resolution burned area products other than the specific one used in our study? We believe that the degree of spatial agreement between active fires and burned area is a useful metric for validation of global burned area products, in addition to the more traditional approach of comparing moderate resolution burned area products with Landsat imagery and geographic information system burn perimeters. A key advantage of this metric is that global patterns can be assessed, and information about performance can be gained in regions where validation data are unavailable. Under ideal conditions, active fires should be within or near the perimeter of burned areas, taking into account the different spatial resolutions of the two products. Divergence between the two products is expected when 1) the active fire product has false positive detections, 2) thermal emissions from non-landscape fire sources have not been adequately screened, or 3) when fire size or fire severity is below the detection limit for the burned area algorithm. We believe that this third condition is the primary driver of the global patterns documented here in Figures 1 and 2, because false detections from MODIS active fires have been quantified and are mostly confined to specific landscape transitions [*Schroeder et al.*, 2008] and because we attempted to carefully screen our database for non-fire hot spots (section 2.1). Furthermore, *Schroeder et al.* [2008] highlight a mechanism by which differential surface heating between vegetated and cleared areas can generate false detections, a problem that was more pronounced with Terra data than Aqua. In this study, the ratio of FC_{out} to FC_{in} was greater for Aqua than Terra. Other types of errors, such as omission errors with the active fire product or commission errors with burned area require diagnosis using other approaches. Even with these limitations, we anticipate that future refinements to both burned area and active fire retrievals will lead to an improved consistency between these two types of data products, and thus the types of comparisons shown here may serve as a useful benchmark for product evaluation.

[63] The spatial and temporal distribution of the fraction of active fires outside of burned area (Figures 1 and 2) provides some guidance for the design of future validation efforts. Important areas for better understanding small fire burned area include Guatemala, Mexico, India, Thailand, Indonesia, Ukraine, China, and the Southeastern U.S. These areas have not been targeted as extensively for field programs, with past efforts often focusing instead on savanna, boreal forest, and Mediterranean ecosystems where fires tend to be larger and to have more persistent effects on surface reflectance [*Justice et al.*, 1996; *Loboda et al.*, 2007; *Roy and Boschetti*, 2009; *Kasischke et al.*, 2011]. Successful field campaigns for small fire estimation will likely require a different investment strategy for project resources as compared with earlier efforts. For example, while Landsat imagery is likely to remain useful, a 16-day repeat cycle (at best) will not capture many burns in areas where the land is being intensively managed for crop or timber products. In this context, international collaboration will be essential, with coordinated targeting of the same region with multiple commercial and

government sensors from several nations over a fire season. Frequent sampling with high spatial resolution imagery is also needed to resolve potential seasonal variations in the efficacy of burned area and active fire products caused by changes in cloud cover, phenology, aerosol loading, and surface soil moisture [e.g., *Laris*, 2005]. Parallel field sampling also is crucial for this class of fires, and requires ground-based measurements of burn perimeters, fire severity, and other forms of land management that might trigger false detections [e.g., *McCarty et al.*, 2009].

4.3. Comparison With Other Regional and Global Fire Studies

[64] Several recent studies have combined active fire and burned area data sets to improve estimates of burned area and carbon emissions [*Roy et al.*, 1999; *Loboda et al.*, 2007; *Boschetti and Roy*, 2009; *Giglio et al.*, 2009; *Roberts et al.*, 2011; *Kaiser et al.*, 2012]. Active fires have been used, for example, to refine thresholds for burned area detection [*Roy et al.*, 1999; *Loboda et al.*, 2007; *Giglio et al.*, 2009], to estimate fuel consumption [*Boschetti and Roy*, 2009], and to more effectively estimate regional-scale biomass burning emissions [*Roberts et al.*, 2011; *Kaiser et al.*, 2012]. An important next step with respect to inter-comparing these different approaches is to reconcile our findings with the fusion approach proposed by *Roberts et al.* [2011]. In that study, the authors found that emissions for Africa increased by only 6% when SEVERI-derived fire radiative energy from fires detected outside of MODIS MCD45A1 burned area was included in their analysis system (they denoted as pathway 1). Here we used a different source for FRP and burned area, and estimate that 34–36% of MODIS-derived FRP was outside of burned areas for Africa (Table 4). A comprehensive analysis of the spatial distribution of MCD45A1 and MCD64A1 burned areas and their relation to MODIS and SEVERI active fire detections will be needed to understand these differences, building on work by *Freeborn et al.* [2009].

[65] In the context of other ongoing burned area and FRE studies, we believe our estimates of small fire impacts on global burned area and biomass burning emissions are likely conservative for four reasons. First, our algorithm reduced but did not eliminate low biases observed for MODIS burned area in several regions of North America and Africa. Second, some small fires are below the detection limit for the MODIS active fire product [*Schroeder et al.*, 2008] and in our opinion, these fires are more likely to occur outside of existing burned area products derived from moderate resolution imagery. Third, our best estimate of global burned area and biomass burning emissions relied on observations from Terra. Use of early afternoon observations from Aqua considerably increased estimates of small fire burned area in our sensitivity study, primarily because proportionately more fires were detected outside of MCD64A1 burned areas. This is consistent with the observation that many agricultural and savanna fires tend to have a more pronounced diurnal cycle than extratropical forest fires, and one that peaks in early afternoon [*Vermote et al.*, 2009; *Mu et al.*, 2011]. As a result, these fires may be more prevalent during the 1:30 pm Aqua overpass than during the 10:30 am Terra overpass. Fourth, as noted in the methods, we attributed all of the observed dNBR changes in equation (4) to burned area. If burn severity is lower (per m^2 of burned area) for small fires outside of MCD64A1 burned areas, then the small fire burned area fractions would have to be even higher to induce the same dNBR change. We note, however, that this latter scenario probably would not translate to higher carbon emissions because lower burn severities per unit of burned area would be expected to have lower levels of fuel consumption.

4.4. Uncertainties

[66] Our study reduced uncertainties in global biomass burning emissions estimates by improving the representation of a key class of fire sizes and by lowering burned area biases in North America and Africa. Nevertheless, uncertainties related to regional and global burned area estimates remain considerable and are related to multiple factors. For example, understory fires in tropical, temperate, and boreal forest biomes probably were not well represented by our approach and further work is needed to quantify these fires and integrate this information with burned area products for other fire types [*Nepstad et al.*, 1999; *Morton et al.*, 2011]. Also, in many areas where biomass burning emissions are important, the seasonal dynamics of fuel properties and cloud cover and their subsequent impact on active fire detection efficiencies and the functioning of burned area algorithms remain poorly understood.

[67] With the approach we developed here, important uncertainties were introduced by the spatial averaging of the 500 m dNBR statistics to the ~1-km resolution of active fire detections, by our assumption of a linear relationship between dNBR changes and sub-pixel burned area, and also by the re-projection and resampling of the active fire swath observations on the MODIS sinusoidal grid that is an integral part of the MOD14A1 product. More specifically, the daily composition thermal anomaly/fire product (MOD14A1) may disproportionately increase FC_{out} from resampling, but this bias also would likely decrease γ. Some of these errors could be avoided in a future reprocessing by using the swath-level fire location product that provides a more precise set of latitude and longitude coordinates for each active fire pixel (MCD14ML), and by filtering this product by a maximum threshold on the across-track scan angle. This latter constraint may reduce spatial smoothing effects that likely occur at high scan angles and also may provide a more representative set of active fire pixels for quantifying dNBR changes inside and outside of burned areas. By combining analysis of Landsat and MODIS in future work, it also may be possible to assess and modify the dNBR-fire size relationship, which is assumed to be constant here in our definition of γ. As a result of the comparisons presented here, additional modifications to the MCD64A1 burned area algorithm are currently being implemented to better represent fires in agriculture and areas of the tropics with dense cloud cover.

[68] For our emissions estimates, important uncertainties exist with respect to the separation of the dNBR changes measured for FC_{out} into burned area and fire severity (combustion completeness) components. To be conservative with respect to our estimates of small fire impacts on burned area, here we assumed the observed dNBR changes were related solely to burned area and as a consequence, we applied the same combustion completeness parameterizations as in GFED3. While we do not believe this assumption led to a high bias in our carbon emissions estimates, additional field observations of burned area perimeters, fuel

loads, and fuel consumption are needed to improve the parameterization of these processes in global models.

5. Conclusions

[69] We developed a unified approach for using information from active fire and 500 m burned area to estimate the contribution of small fires to global burned area and carbon emissions. We found good agreement between the spatial distribution of active fires and burned area in savannas and boreal forests. In other biomes, including croplands, wooded savannas, and tropical forests, we observed many active fires that were outside the perimeter of burned areas. We estimated the area burned for this set of small fires using a novel approach that required tracking the surface reflectance changes of individual active fire detections inside and outside of burned areas, and in nearby control areas. At a global scale, accounting for small fires increased burned area and global carbon emissions by approximately 35%. Sensitivity analyses of key model parameters led to a range of estimates of global burned area increases from small fires, from 24% to 54%. Although preliminary, this analysis indicates that small fires are an important class of global biomass burning emissions and one that needs to be more specifically targeted in future research and validation efforts.

[70] Multiple lines of evidence indicated that our estimates of small fire contributions to burned area and emissions were conservative. Uncertainties remain considerable for this class of fires, and our analysis provided some possible guidance with respect to the design of future validation programs. Specifically, to build reliable regional data sets for small fires, increased emphasis needs to be placed on the development of high temporal and spatial resolution satellite imagery time series (including acquisition and analysis of dozens, if not hundreds of images during a fire season in a specific study area) and simultaneous collection of fire perimeters by mobile ground teams. Key directions for future research including quantifying the contribution of small fires to atmospheric trace gas variability, aerosol radiative forcing, and air quality.

[71] **Acknowledgments.** We thank L. Giglio for careful review of earlier manuscript drafts and for sharing the global MCD64A1 data set for this analysis. We thank Y. Jin for analysis of the fire time series from Portugal. This study was supported by NASA grants NNX11AF96G and NNX10AT83G. B.M.R. received support from an NSF Graduate Fellowship. G.R.v.d.W. received support from the EU FP7 project MACC-II.

References

Amiro, B. D., J. B. Todd, B. M. Wotton, K. A. Logan, M. D. Flannigan, B. J. Stocks, J. A. Mason, D. L. Martell, and K. G. Hirsch (2001), Direct carbon emissions from Canadian forest fires, 1959–1999, *Can. J. For. Res.*, *31*(3), 512–525, doi:10.1139/x00-197.

Aragao, L., and Y. E. Shimabukuro (2010), The incidence of fire in Amazonian forests with implications for REDD, *Science*, *328*(5983), 1275–1278, doi:10.1126/science.1186925.

Arino, O., S. Casadio, and D. Serpe (2012), Global night-time fire season timing and fire count trends using the ATSR instrument series, *Remote Sens. Environ.*, *116*, 226–238, doi:10.1016/j.rse.2011.05.025.

Barbosa, P. M., D. Stroppiana, J. M. Gregoire, and J. M. C. Pereira (1999), An assessment of vegetation fire in Africa (1981–1991), Burned areas, burned biomass, and atmospheric emissions, *Global Biogeochem. Cycles*, *13*(4), 933–950, doi:10.1029/1999GB900042.

Beck, P. S. A., S. J. Goetz, M. C. Mack, H. D. Alexander, Y. F. Jin, J. T. Randerson, and M. M. Loranty (2011), The impacts and implications of an intensifying fire regime on Alaskan boreal forest composition and albedo, *Global Change Biol.*, *17*(9), 2853–2866, doi:10.1111/j.1365-2486.2011.02412.x.

Boschetti, L., and D. P. Roy (2009), Strategies for the fusion of satellite fire radiative power with burned area data for fire radiative energy derivation, *J. Geophys. Res.*, *114*, D20302, doi:10.1029/2008JD011645.

Bowman, D., et al. (2011), The human dimension of fire regimes on Earth, *J. Biogeogr.*, *38*(12), 2223–2236, doi:10.1111/j.1365-2699.2011.02595.x.

Chapin, F. S., P. A. Matson, and H. A. Mooney (2002), *Principles of Terrestrial Ecosystem Ecology*, Springer, New York.

Chen, Y., J. T. Randerson, D. C. Morton, R. S. DeFries, G. J. Collatz, P. S. Kasibhatla, L. Giglio, Y. F. Jin, and M. E. Marlier (2011), Forecasting fire season severity in South America using sea surface temperature anomalies, *Science*, *334*(6057), 787–791, doi:10.1126/science.1209472.

Chuvieco, E., L. Giglio, and C. Justice (2008), Global characterization of fire activity: Toward defining fire regimes from Earth observation data, *Global Change Biol.*, *14*(7), 1488–1502, doi:10.1111/j.1365-2486.2008.01585.x.

Covington, W. W., P. Z. Fule, M. M. Moore, S. C. Hart, T. E. Kolb, J. N. Mast, S. S. Sackett, and M. R. Wagner (1997), Restoring ecosystem health in ponderosa pine forests of the southwest, *J. For.*, *95*(4), 23–29.

Csiszar, I. A., J. T. Morisette, and L. Giglio (2006), Validation of active fire detection from moderate-resolution satellite sensors: The MODIS example in northern Eurasia, *IEEE Trans. Geosci. Remote*, *44*(7), 1757–1764, doi:10.1109/TGRS.2006.875941.

DeWilde, L., and F. S. Chapin (2006), Human impacts on the fire regime of interior Alaska: Interactions among fuels, ignition sources, and fire suppression, *Ecosystems (N. Y.)*, *9*(8), 1342–1353, doi:10.1007/s10021-006-0095-0.

Dozier, J. (1981), A method for satellite identification of surface-temperature fields of subpixel resolution, *Remote Sens. Environ.*, *11*(3), 221–229, doi:10.1016/0034-4257(81)90021-3.

Eidenshink, J., B. Schwind, K. Brewer, Z. Zhu, B. Quayle, and S. Howard (2007), A project for monitoring trends in burn severity, *Fire Ecol.*, *3*(1), 3–21, doi:10.4996/fireecology.0301003.

Ellicott, E., E. Vermote, L. Giglio, and G. Roberts (2009), Estimating biomass consumed from fire using MODIS FRE, *Geophys. Res. Lett.*, *36*, L13401, doi:10.1029/2009GL038581.

Elvidge, C. D., D. Ziskin, K. E. Baugh, B. T. Tuttle, T. Ghosh, D. W. Pack, E. H. Erwin, and M. Zhizhin (2009), A fifteen year record of global natural gas flaring derived from satellite data, *Energies*, *2*(3), 595–622, doi:10.3390/en20300595.

Eva, H., and E. F. Lambin (1998), Remote sensing of biomass burning in tropical regions: Sampling issues and multisensor approach, *Remote Sens. Environ.*, *64*(3), 292–315, doi:10.1016/S0034-4257(98)00006-6.

Field, R. D., G. R. van der Werf, and S. S. P. Shen (2009), Human amplification of drought-induced biomass burning in Indonesia since 1960, *Nat. Geosci.*, *2*(3), 185–188, doi:10.1038/ngeo443.

Freeborn, P. H., M. J. Wooster, W. M. Hao, C. A. Ryan, B. L. Nordgren, S. P. Baker, and C. Ichoku (2008), Relationships between energy release, fuel mass loss, and trace gas and aerosol emissions during laboratory biomass fires, *J. Geophys. Res.*, *113*, D01301, doi:10.1029/2007JD008679.

Freeborn, P. H., M. J. Wooster, G. Roberts, B. D. Malamud, and W. D. Xu (2009), Development of a virtual active fire product for Africa through a synthesis of geostationary and polar orbiting satellite data, *Remote Sens. Environ.*, *113*(8), 1700–1711, doi:10.1016/j.rse.2009.03.013.

Freeborn, P. H., M. J. Wooster, and G. Roberts (2011), Addressing the spatiotemporal sampling design of MODIS to provide estimates of the fire radiative energy emitted from Africa, *Remote Sens. Environ.*, *115*(2), 475–489, doi:10.1016/j.rse.2010.09.017.

French, N. H. F., et al. (2011), Model comparisons for estimating carbon emissions from North American wildland fire, *J. Geophys. Res.*, *116*, G00K05, doi:10.1029/2010JG001469.

Friedl, M. A., et al. (2002), Global land cover mapping from MODIS: Algorithms and early results, *Remote Sens. Environ.*, *83*(1–2), 287–302, doi:10.1016/S0034-4257(02)00078-0.

Friedl, M. A., D. Sulla-Menashe, B. Tan, A. Schneider, N. Ramankutty, A. Sibley, and X. M. Huang (2010), MODIS Collection 5 global land cover: Algorithm refinements and characterization of new datasets, *Remote Sens. Environ.*, *114*(1), 168–182, doi:10.1016/j.rse.2009.08.016.

Giglio, L. (2007), Characterization of the tropical diurnal fire cycle using VIRS and MODIS observations, *Remote Sens. Environ.*, *108*(4), 407–421, doi:10.1016/j.rse.2006.11.018.

Giglio, L. (2010), *MODIS Collection 5 Active Fire Product User's Guide, Version 2.4*, 61 pp., Dep. of Geogr., Univ. of Maryland, College Park, Md.

Giglio, L., J. D. Kendall, and C. J. Tucker (2000), Remote sensing of fires with the TRMM VIRS, *Int. J. Remote Sens.*, *21*(1), 203–207, doi:10.1080/014311600211109.

Giglio, L., J. Descloitres, C. O. Justice, and Y. J. Kaufman (2003), An enhanced contextual fire detection algorithm for MODIS, *Remote Sens. Environ.*, *87*(2–3), 273–282, doi:10.1016/S0034-4257(03)00184-6.

Giglio, L., I. Csiszar, and C. O. Justice (2006a), Global distribution and seasonality of active fires as observed with the Terra and Aqua Moderate Resolution Imaging Spectroradiometer (MODIS) sensors, *J. Geophys. Res.*, *111*, G02016, doi:10.1029/2005JG000142.

Giglio, L., G. R. van der Werf, J. T. Randerson, G. J. Collatz, and P. Kasibhatla (2006b), Global estimation of burned area using MODIS active fire observations, *Atmos. Chem. Phys.*, *6*, 957–974, doi:10.5194/acp-6-957-2006.

Giglio, L., T. Loboda, D. P. Roy, B. Quayle, and C. O. Justice (2009), An active-fire based burned area mapping algorithm for the MODIS sensor, *Remote Sens. Environ.*, *113*(2), 408–420, doi:10.1016/j.rse.2008.10.006.

Giglio, L., J. T. Randerson, G. R. van der Werf, P. S. Kasibhatla, G. J. Collatz, D. C. Morton, and R. S. DeFries (2010), Assessing variability and long-term trends in burned area by merging multiple satellite fire products, *Biogeosciences*, *7*(3), 1171–1186, doi:10.5194/bg-7-1171-2010.

Golding, N., and R. Betts (2008), Fire risk in Amazonia due to climate change in the HadCM3 climate model: Potential interactions with deforestation, *Global Biogeochem. Cycles*, *22*(4), GB4007, doi:10.1029/2007GB003166.

Hansen, M. C., et al. (2008), Humid tropical forest clearing from 2000 to 2005 quantified by using multitemporal and multiresolution remotely sensed data, *Proc. Natl. Acad. Sci. U. S. A.*, *105*(27), 9439–9444, doi:10.1073/pnas.0804042105.

Hély, C., M. Flannigan, Y. Bergeron, and D. McRae (2001), Role of vegetation and weather on fire behavior in the Canadian mixedwood boreal forest using two fire behavior prediction systems, *Can. J. For. Res.*, *31*(3), 430–441, doi:10.1139/x00-192.

Hoelzemann, J. J., M. G. Schultz, G. P. Brasseur, C. Granier, and M. Simon (2004), Global Wildland Fire Emission Model (GWEM): Evaluating the use of global area burnt satellite data, *J. Geophys. Res.*, *109*, D14S04, doi:10.1029/2003JD003666.

Huete, A., K. Didan, T. Miura, E. P. Rodriguez, X. Gao, and L. G. Ferreira (2002), Overview of the radiometric and biophysical performance of the MODIS vegetation indices, *Remote Sens. Environ.*, *83*(1–2), 195–213, doi:10.1016/S0034-4257(02)00096-2.

Ichoku, C., Y. J. Kaufman, L. Giglio, Z. Li, R. H. Fraser, J. Z. Jin, and W. M. Park (2003), Comparative analysis of daytime fire detection algorithms using AVHRR data for the 1995 fire season in Canada: Perspective for MODIS, *Int. J. Remote Sens.*, *24*(8), 1669–1690, doi:10.1080/01431160210144697.

Ito, A., et al. (2008), Can we reconcile differences in estimates of carbon fluxes from land-use change and forestry for the 1990s? *Atmos. Chem. Phys.*, *8*(12), 3291–3310, doi:10.5194/acp-8-3291-2008.

Johnston, F. H., S. B. Henderson, Y. Chen, J. T. Randerson, M. Marlier, R. S. DeFries, P. Kinney, D. M. J. S. Bowman, and M. Brauer (2012), Estimated global mortality attributable to smoke from landscape fires, *Environ. Health Perspect.*, *120*, 695–701, doi:10.1289/ehp.1104422.

Justice, C. O., J. D. Kendall, P. R. Dowty, and R. J. Scholes (1996), Satellite remote sensing of fires during the SAFARI campaign using NOAA advanced very high resolution radiometer, *J. Geophys. Res.*, *101*(D19), 23,851–23,863, doi:10.1029/95JD00623.

Kaiser, J. W., et al. (2012), Biomass burning emissions estimated with a global fire assimilation system based on observations of fire radiative power, *Biogeosciences*, *9*, 527–554, doi:10.5194/bg-9-527-2012.

Kasischke, E. S., and N. H. F. French (1995), Locating and estimating the areal extent of wildfires in Alaskan boreal forests using multiple-season AVHRR NDVI composite data, *Remote Sens. Environ.*, *51*(2), 263–275, doi:10.1016/0034-4257(93)00074-J.

Kasischke, E. S., D. Williams, and D. Barry (2002), Analysis of the patterns of large fires in the boreal forest region of Alaska, *Int. J. Wildland Fire*, *11*(2), 131–144, doi:10.1071/WF02023.

Kasischke, E. S., T. Loboda, L. Giglio, N. H. F. French, E. E. Hoy, B. de Jong, and D. Riano (2011), Quantifying burned area for North American forests: Implications for direct reduction of carbon stocks, *J. Geophys. Res.*, *116*, G04003, doi:10.1029/2011JG001707.

Kaufman, Y. J., C. O. Justice, L. P. Flynn, J. D. Kendall, E. M. Prins, L. Giglio, D. E. Ward, W. P. Menzel, and A. W. Setzer (1998), Potential global fire monitoring from EOS-MODIS, *J. Geophys. Res.*, *103*(D24), 32,215–32,238, doi:10.1029/98JD01644.

Kloster, S., N. M. Mahowald, J. T. Randerson, and P. J. Lawrence (2012), The impacts of climate, land use, and demography on fires during the 21st century simulated by CLM-CN, *Biogeosciences*, *9*(1), 509–525, doi:10.5194/bg-9-509-2012.

Korontzi, S., D. P. Roy, C. O. Justice, and D. E. Ward (2004), Modeling and sensitivity analysis of fire emissions in southern Africa during SAFARI 2000, *Remote Sens. Environ.*, *92*(3), 376–396, doi:10.1016/j.rse.2004.06.023.

Laris, P. S. (2005), Spatiotemporal problems with detecting and mapping mosaic fire regimes with coarse-resolution satellite data in savanna environments, *Remote Sens. Environ.*, *99*(4), 412–424, doi:10.1016/j.rse.2005.09.012.

Lin, H.-W., Y. Jin, L. Giglio, J. A. Foley, and J. T. Randerson (2012), Evaluating greenhouse gas emissions inventories for agricultural burning using satellite observations of active fires, *Ecol. Appl.*, *22*(4), 1345–1364, doi:10.1890/10-2362.1.

Loboda, T., K. J. O'Neal, and I. Csiszar (2007), Regionally adaptable dNBR-based algorithm for burned area mapping from MODIS data, *Remote Sens. Environ.*, *109*(4), 429–442, doi:10.1016/j.rse.2007.01.017.

López Garcia, M. J., and V. Caselles (1991), Mapping burns and natural reforestation using Thematic Mapper data, *Geocarto Int.*, *6*(1), 31–37, doi:10.1080/10106049109354290.

Luo, Y. Q., and E. S. Weng (2011), Dynamic disequilibrium of the terrestrial carbon cycle under global change, *Trends Ecol. Evol.*, *26*(2), 96–104, doi:10.1016/j.tree.2010.11.003.

Marques, S., J. G. Borges, J. Garcia-Gonzalo, F. Moreira, J. M. B. Carreiras, M. M. Oliveira, A. Cantarinha, B. Botequim, and J. M. C. Pereira (2011), Characterization of wildfires in Portugal, *Eur. J. For. Res.*, *130*(5), 775–784, doi:10.1007/s10342-010-0470-4.

Matson, M., and J. Dozier (1981), Identification of subresolution high-temperature sources using a thermal IR sensor, *Photogramm. Eng. Remote Sens.*, *47*(9), 1311–1318.

McCarty, J. L., S. Korontzi, C. O. Justice, and T. Loboda (2009), The spatial and temporal distribution of crop residue burning in the contiguous United States, *Sci. Total Environ.*, *407*(21), 5701–5712, doi:10.1016/j.scitotenv.2009.07.009.

Mollicone, D., H. D. Eva, and F. Achard (2006), Ecology - Human role in Russian wild fires, *Nature*, *440*(7083), 436–437, doi:10.1038/440436a.

Morisette, J. T., L. Giglio, I. Csiszar, and C. O. Justice (2005), Validation of the MODIS active fire product over Southern Africa with ASTER data, *Int. J. Remote Sens.*, *26*(19), 4239–4264, doi:10.1080/01431160500113526.

Morton, D. C., R. S. DeFries, J. Nagol, C. M. Souza, E. S. Kasischke, G. C. Hurtt, and R. Dubayah (2011), Mapping canopy damage from understory fires in Amazon forests using annual time series of Landsat and MODIS data, *Remote Sens. Environ.*, *115*(7), 1706–1720, doi:10.1016/j.rse.2011.03.002.

Mouillot, F., and C. B. Field (2005), Fire history and the global carbon budget: A 1 degrees x 1 degrees fire history reconstruction for the 20th century, *Global Change Biol.*, *11*(3), 398–420, doi:10.1111/j.1365-2486.2005.00920.x.

Mu, M., et al. (2011), Daily and 3-hourly variability in global fire emissions and consequences for atmospheric model predictions of carbon monoxide, *J. Geophys. Res.*, *116*, D24303, doi:10.1029/2011JD016245.

Nepstad, D. C., et al. (1999), Large-scale impoverishment of Amazonian forests by logging and fire, *Nature*, *398*(6727), 505–508, doi:10.1038/19066.

National Interagency Fire Center (NIFC) (2012), Fire information statistics, http://www.nifc.gov/fireInfo/fireInfo_statistics.html, Boise, Idaho.

Page, S. E., F. Siegert, J. O. Rieley, H. D. V. Boehm, A. Jaya, and S. Limin (2002), The amount of carbon released from peat and forest fires in Indonesia during 1997, *Nature*, *420*(6911), 61–65, doi:10.1038/nature01131.

Parisien, M. A., V. S. Peters, Y. H. Wang, J. M. Little, E. M. Bosch, and B. J. Stocks (2006), Spatial patterns of forest fires in Canada, 1980–1999, *Int. J. Wildland Fire*, *15*(3), 361–374, doi:10.1071/WF06009.

Pooter, H., and R. Villar (1997), The fate of acquired carbon in plants: Chemical composition and construction costs, in *Plant Resource Allocation*, edited by F. Bazzaz and J. Grace, pp. 39–72, SPB Acad., The Hague, Netherlands.

Prentice, I. C., D. I. Kelley, P. N. Foster, P. Friedlingstein, S. P. Harrison, and P. J. Bartlein (2011), Modeling fire and the terrestrial carbon balance, *Global Biogeochem. Cycles*, *25*, GB3005, doi:10.1029/2010GB003906.

Prins, E. M., and W. P. Menzel (1992), Geostationary satellite detection of biomass burning in South America, *Int. J. Remote Sens.*, *13*(15), 2783–2799, doi:10.1080/01431169208904081.

Prins, E. M., and W. P. Menzel (1994), Trends in South-American biomass burning detected with the GOES Visible Infrared Spin Scan Radiometer Atmospheric Sounder from 1983–1991, *J. Geophys. Res.*, *99*(D8), 16,719–16,735, doi:10.1029/94JD01208.

PRODES (2012), The Amazon deforestation monitoring project (Programa de cálculo do desflorestamento da Amazônia), www.obt.inpe.br/prodes, Natl. Inst. for Space Res., São José dos Campos, Brazil.

Reid, J. S., et al. (2009), Global monitoring and forecasting of biomass-burning smoke: Description of and lessons from the Fire Locating and Modeling of Burning Emissions (FLAMBE) Program, *IEEE J. Selec. Top. Appl. Earth Obs. Remote Sens.*, *2*(3), 144–162, doi:10.1109/JSTARS.2009.2027443.

Roberts, G., M. J. Wooster, and E. Lagoudakis (2009), Annual and diurnal african biomass burning temporal dynamics, *Biogeosciences*, *6*(5), 849–866, doi:10.5194/bg-6-849-2009.

Roberts, G., M. Wooster, P. H. Freeborn, and W. Xu (2011), Integration of geostationary FRP and polar-orbiter burned area datasets for an enhanced

biomass burning inventory, *Remote Sens. Environ.*, *115*(8), 2047–2061, doi:10.1016/j.rse.2011.04.006.

Roy, D. P., and L. Boschetti (2009), Southern Africa validation of the MODIS, L3JRC, and GlobCarbon burned-area products, *IEEE Trans. Geosci. Remote Sens.*, *47*(4), 1032–1044, doi:10.1109/TGRS.2008.2009000.

Roy, D. P., and T. Landmann (2005), Characterizing the surface heterogeneity of fire effects using multi-temporal reflective wavelength data, *Int. J. Remote Sens.*, *26*(19), 4197–4218, doi:10.1080/01431160500112783.

Roy, D. P., L. Giglio, J. D. Kendall, and C. O. Justice (1999), Multi-temporal active-fire based burn scar detection algorithm, *Int. J. Remote Sens.*, *20*(5), 1031–1038, doi:10.1080/014311699213073.

Roy, D. P., Y. Jin, P. E. Lewis, and C. O. Justice (2005), Prototyping a global algorithm for systematic fire-affected area mapping using MODIS time series data, *Remote Sens. Environ.*, *97*(2), 137–162, doi:10.1016/j.rse.2005.04.007.

Scholes, R. J., J. Kendall, and C. O. Justice (1996), The quantity of biomass burned in southern Africa, *J. Geophys. Res.*, *101*(D19), 23,667–23,676, doi:10.1029/96JD01623.

Schroeder, W., E. Prins, L. Giglio, I. Csiszar, C. Schmidt, J. Morisette, and D. Morton (2008), Validation of GOES and MODIS active fire detection products using ASTER and ETM plus data, *Remote Sens. Environ.*, *112*(5), 2711–2726, doi:10.1016/j.rse.2008.01.005.

Schultz, M. G., A. Heil, J. J. Hoelzemann, A. Spessa, K. Thonicke, J. G. Goldammer, A. C. Held, J. M. C. Pereira, and M. van het Bolscher (2008), Global wildland fire emissions from 1960 to 2000, *Global Biogeochem. Cycles*, *22*, GB2002, doi:10.1029/2007GB003031.

Schwind, B., et al. (2008), Monitoring trends in burn severity: Report on the Pacific Northwest and Pacific Southwest fires (1984 to 2005), http://mtbs.gov/, U.S. Geol. Surv., Washington, D. C.

Seiler, W., and P. J. Crutzen (1980), Estimates of gross and net fluxes of carbon between the biosphere and the atmosphere from biomass burning, *Clim. Change*, *2*(3), 207–247, doi:10.1007/BF00137988.

Silva, J. M. N., J. M. C. Pereira, A. I. Cabral, A. C. L. Sa, M. J. P. Vasconcelos, B. Mota, and J. M. Gregoire (2003), An estimate of the area burned in southern Africa during the 2000 dry season using SPOT-VEGETATION satellite data, *J. Geophys. Res.*, *108*(D13), 8498, doi:10.1029/2002JD002320.

Silva, J. M. N., A. C. L. Sa, and J. M. C. Pereira (2005), Comparison of burned area estimates derived from SPOT-VEGETATION and Landsat ETM plus data in Africa: Influence of spatial pattern and vegetation type, *Remote Sens. Environ.*, *96*(2), 188–201, doi:10.1016/j.rse.2005.02.004.

Simon, M., S. Plummer, F. Fierens, J. J. Hoelzemann, and O. Arino (2004), Burnt area detection at global scale using ATSR-2: The GLOBSCAR products and their qualification, *J. Geophys. Res.*, *109*, D14S02, doi:10.1029/2003JD003622.

Spessa, A., B. McBeth, and C. Prentice (2005), Relationships among fire frequency, rainfall and vegetation patterns in the wet-dry tropics of northern Australia: An analysis based on NOAA-AVHRR data, *Global Ecol. Biogeogr.*, *14*(5), 439–454, doi:10.1111/j.1466-822x.2005.00174.x.

Stroppiana, D., K. Tansey, J. M. Gregoire, and J. M. C. Pereira (2003), An algorithm for mapping burnt areas in Australia using SPOT-VEGETATION data, *IEEE Trans. Geosci. Remote Sens.*, *41*(4), 907–909, doi:10.1109/TGRS.2003.808898.

Tansey, K., et al. (2004), Vegetation burning in the year 2000: Global burned area estimates from SPOT VEGETATION data, *J. Geophys. Res.*, *109*, D14S03, doi:10.1029/2003JD003598.

Tansey, K., J. M. Gregoire, P. Defourny, R. Leigh, J. F. O. Pekel, E. van Bogaert, and E. Bartholome (2008), A new, global, multi-annual (2000–2007) burnt area product at 1 km resolution, *Geophys. Res. Lett.*, *35*(1), L01401, doi:10.1029/2007GL031567.

Tosca, M. G., J. T. Randerson, C. S. Zender, D. L. Nelson, D. J. Diner, and J. A. Logan (2011), Dynamics of fire plumes and smoke clouds associated with peat and deforestation fires in Indonesia, *J. Geophys. Res.*, *116*, D08207, doi:10.1029/2010JD015148.

Tosca, M. G., J. T. Randerson, and C. S. Zender (2012), Global impact of contemporary smoke aerosols from landscape fires on climate and the Hadley circulation, *Atmos. Chem. Phys. Discuss.*, *12*, 28,069–28,108, doi:10.5194/acpd-12-28069-2012.

Turetsky, M. R., E. S. Kane, J. W. Harden, R. D. Ottmar, K. L. Manies, E. Hoy, and E. S. Kasischke (2011), Recent acceleration of biomass burning and carbon losses in Alaskan forests and peatlands, *Nat. Geosci.*, *4*(1), 27–31, doi:10.1038/ngeo1027.

van der Werf, G. R., J. T. Randerson, L. Giglio, N. Gobron, and A. J. Dolman (2008), Climate controls on the variability of fires in the tropics and subtropics, *Global Biogeochem. Cycles*, *22*, GB3028, doi:10.1029/2007GB003122.

van der Werf, G. R., J. T. Randerson, L. Giglio, G. J. Collatz, M. Mu, P. S. Kasibhatla, D. C. Morton, R. S. DeFries, Y. Jin, and T. T. van Leeuwen (2010), Global fire emissions and the contribution of deforestation, savanna, forest, agricultural, and peat fires (1997–2009), *Atmos. Chem. Phys.*, *10*(23), 11,707–11,735, doi:10.5194/acp-10-11707-2010.

Van Wagner, C. E. (1977), Conditions for the start and spread of crown fire, *Can. J. For. Res.*, *7*(1), 23–34, doi:10.1139/x77-004.

van Wagtendonk, J. W., R. R. Root, and C. H. Key (2004), Comparison of AVIRIS and Landsat ETM + detection capabilities for burn severity, *Remote Sens. Environ.*, *92*(3), 397–408, doi:10.1016/j.rse.2003.12.015.

Vermote, E., E. Ellicott, O. Dubovik, T. Lapyonok, M. Chin, L. Giglio, and G. J. Roberts (2009), An approach to estimate global biomass burning emissions of organic and black carbon from MODIS fire radiative power, *J. Geophys. Res.*, *114*, D18205, doi:10.1029/2008JD011188.

Wang, D., D. C. Morton, J. F. Masek, A. Wu, J. Nagol, X. Xiong, R. Levy, E. Vermote, and R. Wolfe (2012), Impact of sensor degradation on the MODIS NDVI time series, *Remote Sens. Environ.*, *119*, 55–61, doi:10.1016/j.rse.2011.12.001.

Wiedinmyer, C., B. Quayle, C. Geron, A. Belote, D. McKenzie, X. Y. Zhang, S. O'Neill, and K. K. Wynne (2006), Estimating emissions from fires in North America for air quality modeling, *Atmos. Environ.*, *40*(19), 3419–3432, doi:10.1016/j.atmosenv.2006.02.010.

Wooster, M. J., B. Zhukov, and D. Oertel (2003), Fire radiative energy for quantitative study of biomass burning: Derivation from the BIRD experimental satellite and comparison to MODIS fire products, *Remote Sens. Environ.*, *86*(1), 83–107, doi:10.1016/S0034-4257(03)00070-1.

Wooster, M. J., G. Roberts, G. L. W. Perry, and Y. J. Kaufman (2005), Retrieval of biomass combustion rates and totals from fire radiative power observations: FRP derivation and calibration relationships between biomass consumption and fire radiative energy release, *J. Geophys. Res.*, *110*, D24311, doi:10.1029/2005JD006318.

Xu, W., M. J. Wooster, G. Roberts, and P. Freeborn (2010), New GOES imager algorithms for cloud and active fire detection and fire radiative power assessment across North, South and Central America, *Remote Sens. Environ.*, *114*(9), 1876–1895, doi:10.1016/j.rse.2010.03.012.

Yevich, R., and J. A. Logan (2003), An assessment of biofuel use and burning of agricultural waste in the developing world, *Global Biogeochem. Cycles*, *17*(4), 1095, doi:10.1029/2002GB001952.

Zhang, X. Y., and S. Kondragunta (2008), Temporal and spatial variability in biomass burned areas across the USA derived from the GOES fire product, *Remote Sens. Environ.*, *112*(6), 2886–2897, doi:10.1016/j.rse.2008.02.006.

Auxiliary Material for

Global burned area and biomass burning emissions from small fires

J. T. Randerson, Y. Chen, and B. M. Rogers
Department of Earth System Science, University of California, Irvine, California, USA

G. R. van der Werf
Faculty of Earth and Life Sciences, VU University Amsterdam, Amsterdam, Netherlands

D. C. Morton
NASA Goddard Space Flight Center, Biospheric Sciences Branch, Greenbelt, Maryland, USA

Randerson, J. T., Y. Chen, G. R. van der Werf, B. M. Rogers, and D. C. Morton (2012), Global burned area and biomass burning emissions from small fires, J. Geophys. Res., 117, G04012, doi:10.1029/2012JG002128.

Introduction

This auxiliary material contains six items: one table that describes results from our sensitivity analysis in which we modified key assumptions or remote sensing data sets used in our analysis; and five supplementary figures. The five figures describe a flow diagram for our methods approach and comparisons of our burned area estimates from small fires with observations from North America and Portugal. Individual captions for the table and the figures are given below.

Table S1. Summary of sensitivity studies conducted to estimate uncertainties. The baseline case shows the 2010 annual mean burned area for the original BAMCD64A1 product and the impact of adding small fire burned area (BAtotal) in units of Mha/yr. Subsequent columns show the impact on BAtotal of one of the five sensitivity tests described in the main text. The BAsen column reflects the impact of the sensitivity test on BAtotal and the %change column shows the percent change for each region relative to BAtotal. The five sensitivity tests are 1) replacing the surface reflectance product used to compute the difference normalized burn ratio (dNBR) from the 16-day MOD13A1 composition with the 8-day MOD09A1 product, 2) replacing the dNBR control constructed from nearby areas with a control constructed using the same pixels but from the previous year (temporal dNBR control), 3) computing FCin, FCout, and alpha in equation 2 using Aqua instead of Terra thermal anomaly/active fire observations, 4) the same as test 3, but also using these same Aqua observations to compute gamma, and 5) using only higher quality Terra active fires rather than all Terra active fires in the baseline case.

Column 1.1. “Region”, no units, continental-scale region defined in the Figure 1 caption in the main text.

Column 1.2. “BAMCD64A1”, Mha/yr, burned area during 2010 derived from the MODIS MCD64A1 product in the main text. This is the baseline simulation.

Column 1.3. "BATOTAL", Mha/yr, total burned area during 2010 derived from the sum of the MODIS MCD64A1 product and small fire burned area (BAsf) defined in the main text. This is the total burned area for the baseline simulation.

Column 1.4. "SR_BAsen", Mha/yr, total burned area during 2010 derived from the sensitivity study in which the surface reflectance product used to compute the difference normalized burn ratios was replaced with MOD09A1.

Column 1.5. "SR_%change", % (percent change), the percent change in small fire burned area relative to the baseline case, for the sensitivity study in which the surface reflectance product used to compute the difference normalized burn ratios was replaced with MOD09A1.

Column 1.6. "TC_BAsen", Mha/yr, total burned area during 2010 derived from the sensitivity study in which the difference normalized burn ratio for the control region was estimated using data from the previous year. Known as the temporal control case.

Column 1.7. "TC_%change", % (percent change), the percent change in small fire burned area relative to the baseline case, for the sensitivity study in which the difference normalized burn ratio for the control region was estimated using data from the previous year.

Column 1.8. "AQ_BAsen", Mha/yr, total burned area during 2010 derived from the sensitivity study in which Aqua was used to derive FCout, FCin, and alpha.

Column 1.9. "AQ_%change", % (percent change), the percent change in small fire burned area relative to the baseline case, for the sensitivity study in which Aqua was used to derive FCout, FCin, and alpha.

Column 1.10. "AQg_BAsen", Mha/yr, total burned area during 2010 derived from the sensitivity study in which Aqua was used to derive FCout, FCin, alpha, and gamma.

Column 1.11. "AQg_%change",% (percent change), the percent change in small fire burned area relative to the baseline case, for the sensitivity study in which Aqua was used to derive FCout, FCin, alpha, and gamma.

Column 1.12. "HQ_BAsen", Mha/yr, total burned area during 2010 derived from the sensitivity study in which only active fires with moderate or high quality from Terra were used to derive FCout, FCin, alpha, and gamma.

Column 1.13. "HQ_%change", % (percent change), the percent change in small fire burned area relative to the baseline case, for the sensitivity study in which only active fires with moderate or high quality from Terra were used to derive FCout, FCin, alpha, and gamma.

Table S1. Summary of sensitivity studies conducted to estimate uncertainties.

Region	BAM CD64A1	BA total	SR_ Basen	SR_ %change	TC_ BAsen	TC_ %change	AQ_ BAsen	AQ_ %change	AQg_ BAsen	AQg_ %change	HQ_ BAsen	HQ_ %change
BONA	2.9	3.2	3.1	-42.4	3.3	21.2	3.3	18.2	3.3	21.2	3.3	15.2
TENA	1.1	2.7	2.5	-14	2.3	-25	3	18.9	3	17.1	3	15.2
CEAM	0.7	3.2	2.7	-19.4	3.2	-0.8	3.6	15.1	3	-9.5	3.3	3.6
NHSA	2.3	4.3	4.7	17.9	4.4	6	5.1	40.8	4.8	23.9	4.9	29.4
SHSA	32.8	43.1	45.7	25.3	45	18.1	45.7	25	45.4	22.6	43.7	5.5
EURO	0.3	0.8	0.7	-28.3	0.8	3.8	0.8	-1.9	0.7	-13.2	0.8	0
MIDE	1.1	2.8	2.2	-34	3.4	40.1	2.7	-4.9	2.6	-9.9	2.9	6.8
NHAF	97.1	128.5	124.3	-13.4	127.8	-2.2	143.2	46.8	147.3	59.9	129.5	3.2
SHAF	141.6	184.6	177	-17.7	168.7	-37	201.5	39.3	215.7	72.3	187.1	5.9
BOAS	4	7.7	4.6	-84.4	6.1	-44.7	8.1	10.5	7.6	-1.9	7.9	5.1
CEAS	13.8	23.8	19.5	-42.6	20.2	-36.3	25.2	14.9	25.2	14.6	24.4	6.5
SEAS	10.3	17	15.8	-17.5	18.9	28.3	19.4	35.4	19.9	42	17.3	3.8
EQAS	0.2	1.3	0.9	-29.9	0.9	-34.6	1.6	36.4	1.4	13.1	1.8	54.2
AUST	16.1	18	18.5	26.2	18.1	3.7	19	53.9	18.7	37.2	18.1	3.7
Globe	324.2	440.9	422.2	-16.1	423	-15.4	482.2	35.4	498.6	49.4	447.8	5.9

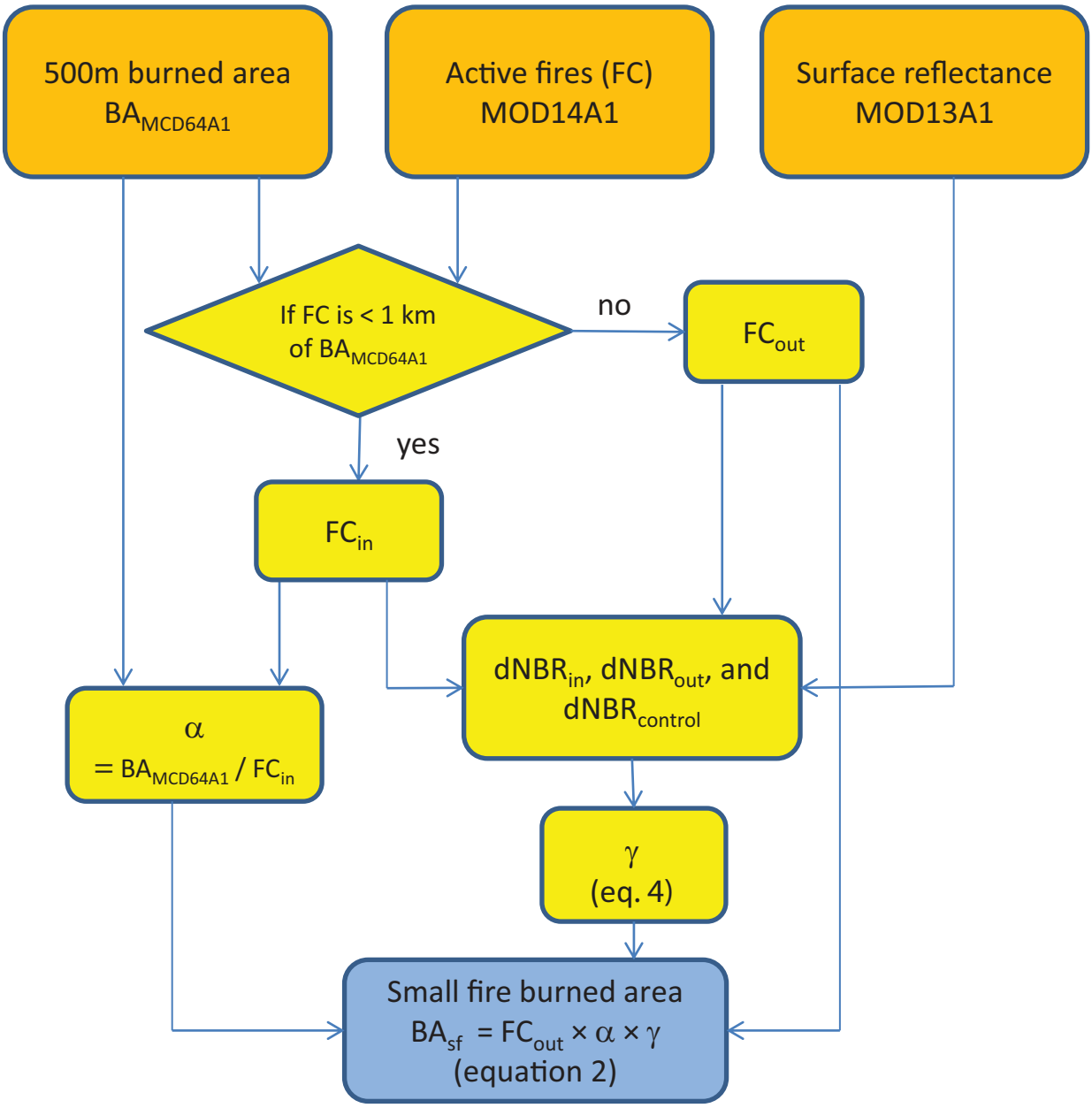

Figure S1. Flow diagram for estimating small fire burned area (BAsf) when MODIS burned area tiles (MOD64A1) were available. The three primary MODIS datasets used in the calculation are shown at the top of the figure in orange. Intermediate calculations are in yellow, and the final small fire burned area product is shown in blue. The 500m burned area product BAMCD64A1 was combined with the daily composition thermal anomaly/fire product MOD14A1 to identify active fires (FC) inside (FCin) and outside (FCout) of BA MCD64A1 polygons. FCin was then used with the BAMCD64A1 product to compute the ? term in the small fire equation: the ratio of burned area per active fire. FCin and FCout were used in parallel to compute difference normalized burn ratio (dNBR) values for the two different sets of active fires (dNBRin, dNBRout), along with this quantity for unburned control areas (dNBRcontrol). Together, the three sets of dNBR were used to estimate the gamma parameter which represents the degree to which alpha is reduced for computing burned area from FCout, to take into account that these active fires probably corresponded to smaller fire scars. In all of the intermediate and final steps, averaging was performed and separate calculations were made for alpha and gamma as a function of seasonal period, year, continental region, and aggregated vegetation class. FCout was allowed to vary each month and in each 0.25 degree grid cell in equation 2.

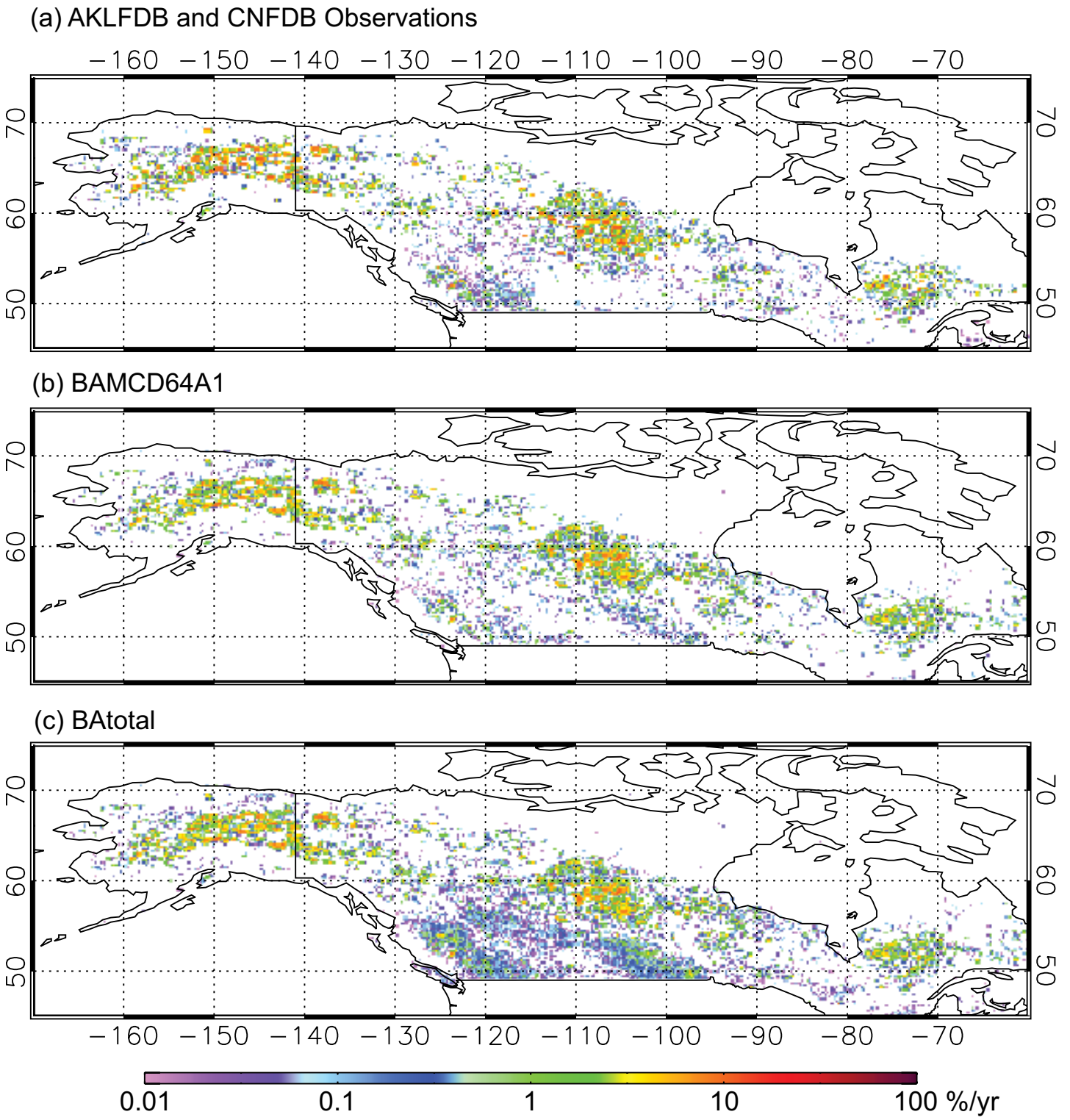

Figure S2. Burned area from the point version of the AKLFDB and CNFDB datasets averaged during 2002-2010 compared to the MODIS burned area products BAMCD64A1 and BAtotal (units are % of each 0.25 degree grid cell per year averaged during 2002-2010). Including small fires in BAtotal increased MODIS burned area across Alberta and British Columbia, and the wheat belt in southern Saskatchewan.

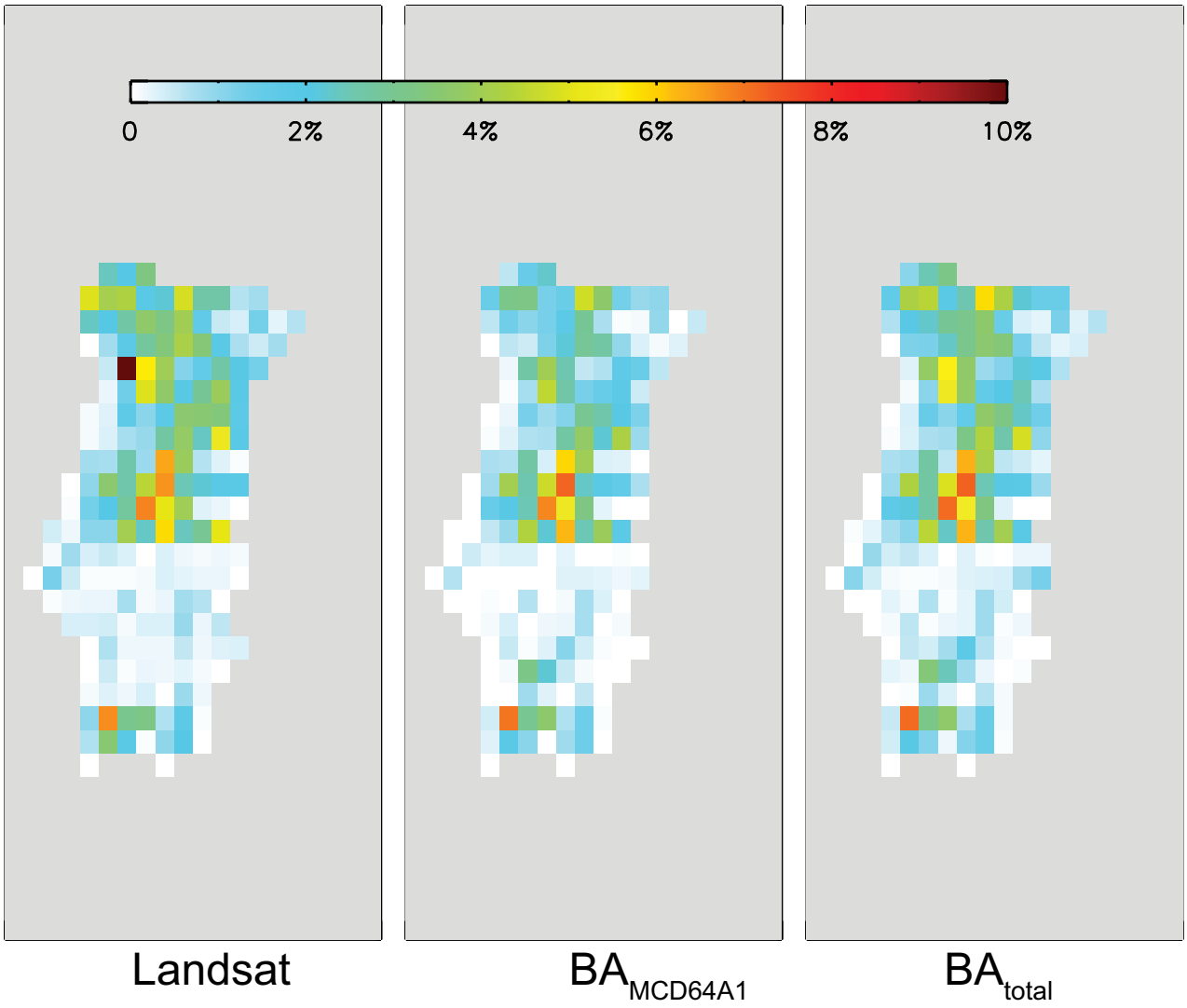

Figure S3. Burned area for Portugal (%/yr) derived from Landsat imagery from the Portugal National Forest service (www.afn.min-agricultura.pt/portal/dudf/cartografia/cartograf-areas-ardidas-1990-2009). Small fire burned area (BAsf) did not vary as much as the observations or BA MCD64A1, and increased the total MODIS burned area in each year by a small amount.

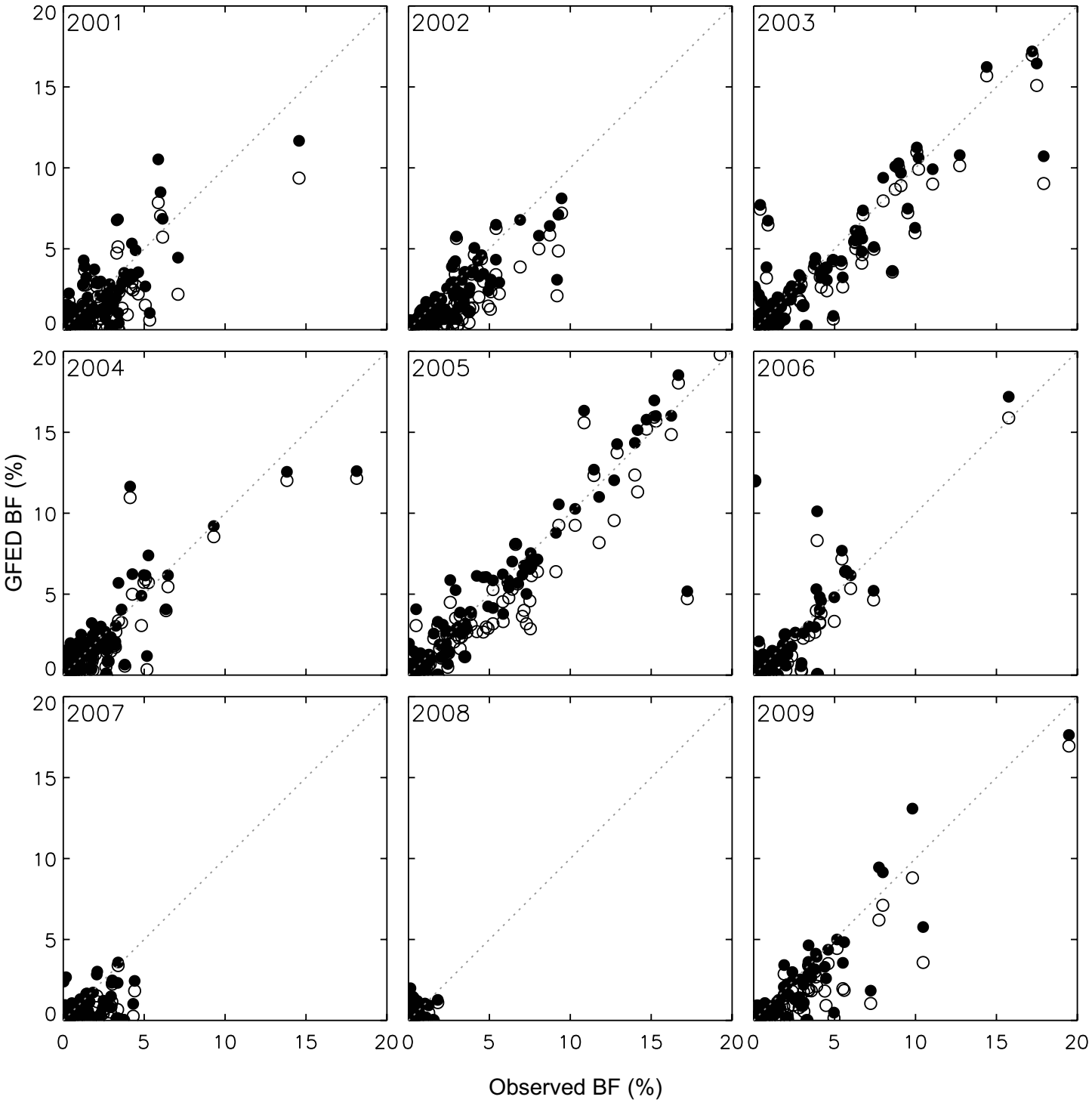

Figure S4. Annual mean burned area from Portugal during 2002-2010 compared to the MODIS burned area products BAMCD64A1 and BAtotal. Including small fires in BAtotal increased MODIS burned area in the northern part of the country and improved the agreement between MODIS burned area and the national inventory derived from Landsat.

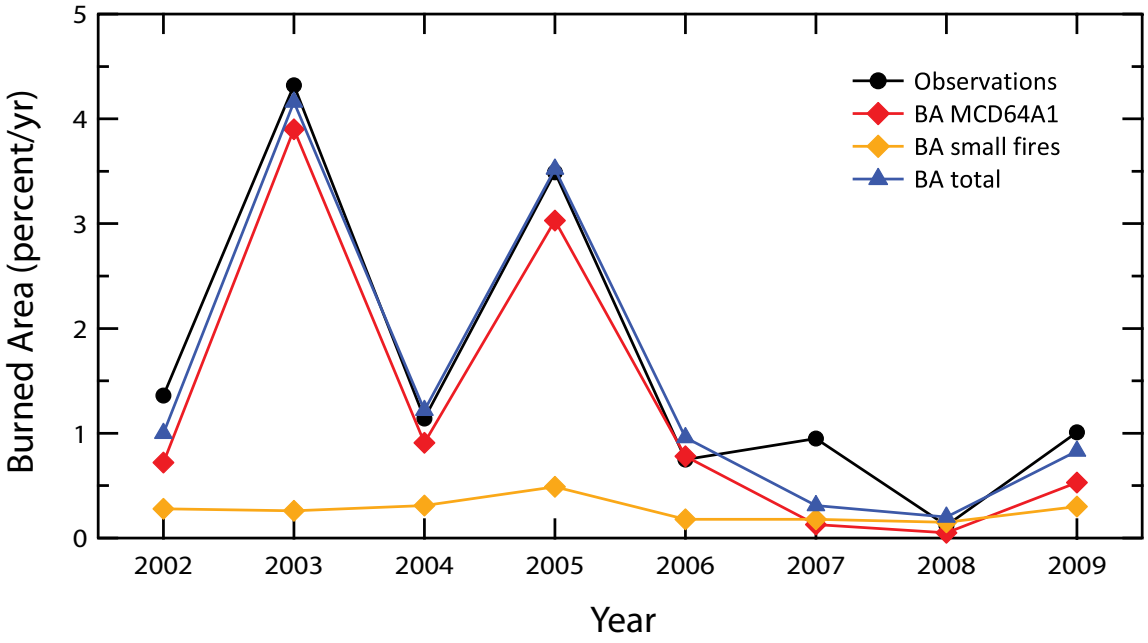

Figure S5. Burned area from a national polygon fire dataset from Portugal during 2001-2010 (observed BF) compared to the MODIS burned area products BAMCD64A1 (open circles) and BAtotal (closed circles). Each point is the burned area fraction of a 0.25 degrees grid cell within Portugal. Including small fires in BAtotal increased the correlation coefficient (r) of the regression line in all of the years shown, except 2004.